CrossMark

J. Plasma Phys. (2021), *vol*. 87, 835870201 © The Author(s), 2021.
Published by Cambridge University Press
doi:10.1017/S0022377821000246

Long-term dynamics driven by resonant wave–particle interactions: from Hamiltonian resonance theory to phase space mapping

Anton V. Artemyev[1,2,†], **Anatoly I. Neishtadt**[2,3], **Alexei. A. Vasiliev**[2], **Xiao-Jia Zhang**[1], **Didier Mourenas**[4] **and Dmitri Vainchtein**[2,5]

[1]Institute of Geophysics and Planetary Physics, UCLA, Los Angeles, CA 90095, USA

[2]Space Research Institute of the Russian Academy of Sciences (IKI), 84/32 Profsoyuznaya Str., Moscow 117997, Russia

[3]Department of Mathematical Sciences, Loughborough University, Loughborough LE11 3TU, UK

[4]Laboratoire Matière sous Conditions Extrêmes, Paris-Saclay University, CEA, Bruyères-le-Châtel 91190, France

[5]Nyheim Plasma Institute, Drexel University, Camden, NJ 08103, USA

(Received 5 November 2020; revised 21 February 2021; accepted 23 February 2021)

In this study we consider the Hamiltonian approach for the construction of a map for a system with nonlinear resonant interaction, including phase trapping and phase bunching effects. We derive basic equations for a single resonant trajectory analysis and then generalize them into a map in the energy/pitch-angle space. The main advances of this approach are the possibility of considering effects of many resonances and to simulate the evolution of the resonant particle ensemble on long time ranges. For illustrative purposes we consider the system with resonant relativistic electrons and field-aligned whistler-mode waves. The simulation results show that the electron phase space density within the resonant region is flattened with reduction of gradients. This evolution is much faster than the predictions of quasi-linear theory. We discuss further applications of the proposed approach and possible ways for its generalization.

Key words: space plasma physics, plasma waves

1. Introduction

The resonant wave–particle interaction is known to be one of the main drivers of dynamics of such space plasma systems as planetary radiation belts (e.g. Thorne 2010; Menietti *et al.* 2012), collisionless shock waves (e.g. Balikhin *et al.* 1997; Wilson *et al.* 2007, 2012; Wang *et al.* 2020), auroral acceleration region (e.g. Chaston *et al.* 2008; Watt & Rankin 2009; Mauk *et al.* 2017) and solar wind (e.g. Krafft & Volokitin 2016; Kuzichev *et al.* 2019; Roberg-Clark *et al.* 2019; Tong *et al.* 2019; Yoon *et al.* 2019). The classical quasi-linear theory (Drummond & Pines 1962; Vedenov, Velikhov & Sagdeev 1962) and its generalizations for inhomogeneous plasma systems (Ryutov 1969; Lyons & Williams 1984) describe well charged particle resonant interaction with

† Email address for correspondence: aartemyev@igpp.ucla.edu

https://doi.org/10.1017/S0022377821000246 Published online by Cambridge University Press

low-amplitude broadband waves (Karpman 1974; Shapiro & Sagdeev 1997; Tao *et al.* 2012*a*; Camporeale & Zimbardo 2015; Allanson *et al.* 2020).

One of the important examples of the application of the quasi-linear theory is the Earth radiation belt models that describe energetic electron acceleration and losses due to resonances with electromagnetic whistler-mode waves and electromagnetic ion cyclotron (EMIC) waves (see reviews Millan & Thorne (2007), Shprits *et al.* (2008), Nishimura *et al.* (2010), Thorne *et al.* (2010), Ni *et al.* (2016) and references therein). Moreover, the natural inhomogeneity of the background magnetic field and plasma density in the radiation belts can significantly weaken the conditions of applicability of the quasi-linear theory (Solovev & Shkliar 1986; Albert 2001, 2010). However, this theory meets difficulties in describing resonances with sufficiently intense waves (Shapiro & Sagdeev 1997), when the nonlinear effects of phase trapping and phase bunching become important (Omura *et al.* 1991; Shklyar & Matsumoto 2009; Albert, Tao & Bortnik 2013; Artemyev *et al.* 2018*a*). Indeed, sufficiently intense whistler-mode waves are frequently observed in the radiation belts (Cattell *et al.* 2008; Wilson *et al.* 2011; Agapitov *et al.* 2014) and contribute significantly to wave statistics (Zhang *et al.* 2018, 2019; Tyler *et al.* 2019). Theoretically, phase trapping and bunching (also called nonlinear scattering) effects are responsible for fast acceleration (e.g. Demekhov *et al.* 2006, 2009; Omura, Furuya & Summers 2007; Hsieh & Omura 2017*a*; Hsieh, Kubota & Omura 2020) and losses (e.g. Kubota, Omura & Summers 2015; Kubota & Omura 2017; Grach & Demekhov 2020) of energetic electrons and for the generation of coherent whistler-mode waves (Omura, Katoh & Summers 2008; Demekhov 2011; Nunn & Omura 2012; Omura, Nunn & Summers 2013; Katoh 2014; Tao 2014; Katoh & Omura 2016). There are many observational evidences of such nonlinear resonant wave generation (Titova *et al.* 2003; Cully *et al.* 2011; Tao *et al.* 2012*b*; Mourenas *et al.* 2015) and of the related electron acceleration/losses (e.g. Foster *et al.* 2014; Agapitov *et al.* 2015*b*; Mourenas *et al.* 2016*a*; Chen *et al.* 2020; Gan *et al.* 2020*b*).

The quasi-linear diffusion theory describes a sufficiently weak scattering in energy/pitch-angle space and operates with a Fokker–Planck diffusion equation for the charged particle distribution function (Andronov & Trakhtengerts 1964; Kennel & Engelmann 1966; Lerche 1968). In contrast to this description, the nonlinear phase trapping assumes a fast transport in energy/pitch-angle space (e.g. Furuya, Omura & Summers 2008; Artemyev *et al.* 2014*b*), when even a single resonant interaction changes significantly the electron's energy/pitch-angle (e.g. Albert *et al.* 2013; Artemyev *et al.* 2018*a*). This essentially non-diffusive process cannot be directly included into the Fokker–Planck equation. One possible approach is the construction of an operator that would describe fast charged particle jumps in the energy/pitch-angle; this operator can be constructed with the numerical (test-particle) approach (e.g. Hsieh & Omura 2017*b*; Zheng, Chen & Zhu 2019) or with the analytical calculation of jumps' probabilities (e.g. Vainchtein *et al.* 2018). The main advantage of this approach is the inclusion of an almost arbitrary (as realistic as needed) wave spectrum and characteristics (e.g. wave modulation and frequency drifts, see Kubota & Omura (2018), Artemyev, Vasiliev & Neishtadt (2019*b*) and Hiraga & Omura (2020)). The main disadvantages are an accumulation of numerical errors with running time, and the almost intractable fine details of the energy/pitch-angle space binning needed to simultaneously resolve large jumps due to trapping and small changes due to drift/diffusion.

An alternative approach to the construction of such an operator is a generalization of the Fokker–Planck equation to include effects of phase trapping and phase bunching (Solovev & Shkliar 1986; Artemyev *et al.* 2016*b*, 2017). This approach is based on a fine balance of trappings and bunchings for a single wave system (e.g. Shklyar 2011; Artemyev, Neishtadt

https://doi.org/10.1017/S0022377821000246 Published online by Cambridge University Press

& Vasiliev 2019*a*). The main advantage of this approach is that the evolution of a charged particle distribution function can be investigated in arbitrary detail in the presence of phase trapping, phase bunching and diffusion (e.g. Artemyev *et al.* 2018*b*, 2019*a*). The main disadvantage is that there is no straightforward generalization of this approach for multiwave (multiresonance) systems. A single-wave resonance results in charged particle transport in the energy/pitch-angle space along one-dimensional (1-D) curves, so-called resonance surface curves (e.g. Lyons & Williams 1984; Summers, Thorne & Xiao 1998), and the Fokker–Planck equation with trapping was derived for such a quasi-1-D system (Artemyev *et al.* 2016*b*).

Another alternative for the description of charged particle distribution evolution driven by nonlinear wave–particle interaction (phase trapping and bunching) is the mapping technique that describes the characteristics of the Fokker–Planck equation (Van Kampen 2003). The classical example of this approach is the Chirikov map (Chirikov 1979), which describes particle diffusion and is widely used for systems with wave–particle resonances (e.g. Vasilev *et al.* 1988; Zaslavskii *et al.* 1989; Benkadda, Sen & Shklyar 1996; Khazanov, Tel'nikhin & Kronberg 2013, 2014). Such a map has been constructed for a single-wave system with phase trapping and phase bunching effects (Artemyev, Neishtadt & Vasiliev 2020*b*). In this study we show the generalization of this map for a multiresonance system.

We consider a strong magnetic field system, where charged particle motion is very gyrotropic and magnetic moments are well-conserved away from the resonances. Thus, three-dimensional velocity space can be reduced to 2-D energy/pitch-angle space. The mapping for this space should describe 2-D charged particle motion due to energy/pitch-angle jumps with the time intervals between jumps equal to the interval between passages through the resonances. Diffusive jumps (with zero mean values) and jumps driven by nonlinear phase bunching and phase trapping depend on the resonant phase φ_R, i.e. a variable proportional to the particle gyrophase, which changes fast. In low wave intensity systems this phase is randomly distributed over the entire ($\varphi_R \in [0, 2\pi]$) range, and the phase dependence $\sim \sin\varphi_R$ can be directly included into the map (Vasilev *et al.* 1988; Zaslavskii *et al.* 1989; Benkadda *et al.* 1996; Khazanov *et al.* 2013, 2014). The phase bunching and phase trapping operate in certain φ_R ranges (e.g. Albert 1993; Itin, Neishtadt & Vasiliev 2000; Grach & Demekhov 2020), whereas jumps depend on φ_R quite non-monotonically (see Artemyev *et al.* 2014*a*, 2018*a*). However, due to phase randomization between two successive resonances (see the appendix in Artemyev *et al.* (2020*b*)), the phase dependence can be reduced to a simplified determination of ranges corresponding to phase trapping $\varphi_R \in [0, 2\pi\Pi]$ and phase bunching $\varphi_R \in [\Pi, 2\pi]$ where $\Pi < 1$ is the probability of trapping (see, e.g. Artemyev *et al.* 2018*a*). The phase gain between two resonances is a large value depending on particle energy and pitch-angle, but this dependence can be omitted in the leading approximation (see discussion in Artemyev *et al.* (2020*b*)). Therefore, in this study we consider charged particle transport in the energy/pitch-angle space due to nonlinear resonant interaction under assumption of resonant phase randomization (limitations of this assumption have been studied in Artemyev, Neishtadt & Vasiliev (2020*a*)).

The paper structure includes a description of the basic system properties and examples of multiresonant systems observed in the Earth's radiation belts (§ 1). We present three examples: with two whistler-mode waves providing two cyclotron resonances; with one oblique whistler-mode wave providing cyclotron and Landau resonances; and with one whistler-mode wave and one EMIC wave providing two different cyclotron resonances. Then we focus on the first example and construct the map for this system (§ 2). Theoretical results derived from this map are verified with test particle simulations. At the end of the

https://doi.org/10.1017/S0022377821000246 Published online by Cambridge University Press

paper we discuss the constructed map and possible extensions of the proposed approach (§ 3).

2. Basic system properties

The Hamiltonian of a relativistic charged particle (e.g. an electron with rest mass m_e and charge $-e$) moving in the 2-D inhomogeneous magnetic field of the Earth dipole and interacting with electromagnetic waves (in the low amplitude limit with the wave energy U_w much smaller than electron energy $\sim m_{ec}^2$, where c is the speed of light) can be written as (e.g. Albert *et al.* 2013; Artemyev *et al.* 2018*b*)

$$\left.\begin{aligned} H &= m_e c^2\gamma + U_w(s, I_x)\sin(\phi \pm n\psi), \\ \gamma &= \sqrt{1 + \frac{p_\parallel^2}{m_e^2 c^2} + \frac{2I_x\Omega_{\rm ce}}{m_e c^2}}, \end{aligned}\right\} \tag{2.1}$$

where two pairs of conjugate variables are $(s, p_\parallel)$ (the field-aligned coordinate and momentum) and (ψ, I_x) (gyrophase and momentum $I_x = c\mu/e$; μ is the classical magnetic moment). The electron gyrofrequency $\Omega_{\rm ce} = eB_0/m_e c$ is determined by the background magnetic field $B_0(s)$, given by, e.g. the reduced dipole model (Bell 1984). The sign $\pm$ in front of ψ is determined by the wave polarization: $+$ for whistler-mode waves interacting with electrons and $-$ for EMIC waves interacting with electrons. The resonance number is $n = 0, \pm 1, \pm 2 \ldots$. The wavevector $\mathbf{k} = (k_\parallel(\omega, s), k_\perp(\omega, s))$ is given by a cold plasma dispersion equation (Stix 1962) for a constant wave frequency ω (i.e. $\partial\phi/\partial s = k_\parallel$, $\partial\phi/\partial t = \omega$). For a finite angle $\theta = \arctan(k_\perp/k_\parallel)$ between the wavevector and the background magnetic field, the wave amplitude in Hamiltonian (2.1) takes the form (Albert 1993; Tao & Bortnik 2010; Nunn & Omura 2015; Artemyev *et al.* 2018*b*)

$$\begin{aligned} U_w = &\sqrt{\frac{2I_x\Omega_{\rm ce}}{m_e c^2}}\frac{eB_w}{k}\sum_{\pm}\frac{\cos\theta \pm C_1}{2\gamma}J_{n\pm1}\left(\sqrt{\frac{2I_x k^2}{m_e\Omega_{\rm ce}}}\sin\theta\right) \\ &+ \frac{eB_w}{k}\left(\frac{p_\parallel}{\gamma m_e c} + C_2\right)J_n\left(\sqrt{\frac{2I_x k^2}{m_e\Omega_{\rm ce}}}\sin\theta\right)\sin\theta, \end{aligned} \tag{2.2}$$

where B_w is the wave magnetic field amplitude, $C_{1,2}$ are functions of wave dispersion and θ, and J_n are Bessel functions. Equation (2.2) shows that for field-aligned waves $\theta = 0$ there is only one cyclotron resonance $n = -1$: $U_w = \sqrt{2I_x\Omega_{\rm ce}/m_e c^2}eB_w/k\gamma$ (with $C_1 = 1$ for $\theta = 0$, see Tao & Bortnik (2010)). For oblique wave propagation $\theta \neq 0$ the whole set of resonances with different values of n is present.

2.1. *Field-aligned whistler waves*

Let us start with the system of two field-aligned whistler waves with the Hamiltonian

$$H = m_e c^2\gamma + \sqrt{\frac{2I_x\Omega_{\rm ce}}{m_e c^2}}\frac{e}{\gamma}\sum_{i=0,1}\frac{B_{w,i}}{k_i}\sin(\phi_i + \psi), \tag{2.3}$$

where $\partial\phi_i/\partial s = k_i = k_i(\omega_i, s)$ with the two different wave frequencies ω_i. Figure 1 shows an example of such system observations. The THEMIS spacecraft measure waves within the whistler-mode frequency range ($f \in [0.1, 1]f_{\rm ce}$; $f_{\rm ce} = \Omega_{\rm ce}/2\pi$): there are two clear

https://doi.org/10.1017/S0022377821000246 Published online by Cambridge University Press

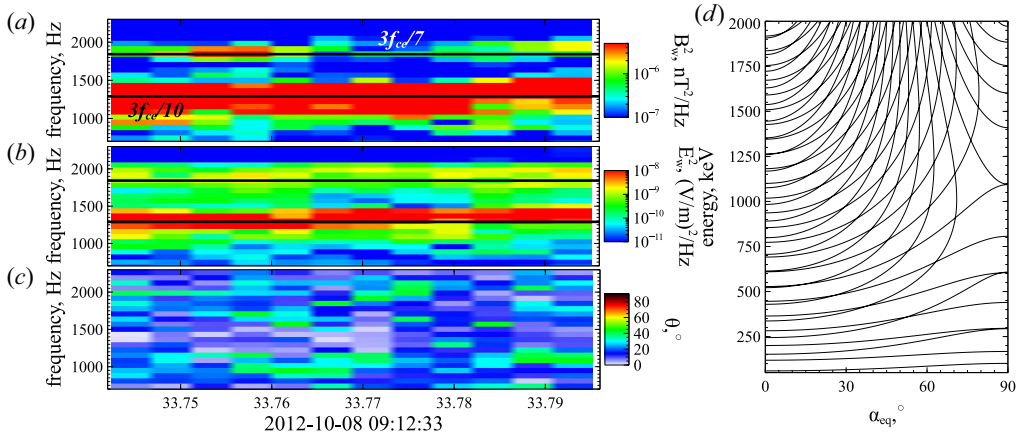


FIGURE 1. Observational example of two whistler-mode waves by Van Allen Probe A (Mauk *et al.* 2013): magnetic field spectrum (*a*) and electric field spectrum (*b*) are obtained from EMFISIS measurements (Kletzing *et al.* 2013), wave-normal angle (*c*) is estimated using Mean's method (Means 1972). Resonance curves for the system with two observed whistler-mode waves (*d*).

maxima in the magnetic and electric field spectra at $f \sim f_{ce}/4$ and $f \sim 3f_{ce}/8$ (see panels (*a*) and (*b*)). Both waves propagate along the background magnetic field: panel (*c*) shows θ as a function of the frequency. These double-peak spectra are quite typical for whistler-mode waves in the inner magnetosphere (see, e.g. Meredith *et al.* 2007; Crabtree *et al.* 2017; Ma *et al.* 2017; He *et al.* 2020; Yu *et al.* 2020; Zhang *et al.* 2020*b*).

To study electron energy/pitch-angle variation in the system with Hamiltonian (2.3), we follow the standard procedure (Neishtadt & Vasiliev 2006; Neishtadt 2014) and introduce the wave phases as new canonical variables, $\varphi_i = \phi_i + \psi$, with the generating function

$$W = sP + \left(\int k_0(\tilde{s})\,\mathrm{d}\tilde{s} - \omega_0 t + \psi\right) I_0 + \left(\int k_1(\tilde{s})\,\mathrm{d}\tilde{s} - \omega_1 t + \psi\right) I_1. \tag{2.4}$$

This function gives new variables: $P = p - k_0 I_0 - k_1 I_1$, $S = s$ (we keep s notation), $I_x = I_0 + I_1$ and new Hamiltonian $H_I = H + \partial W/\partial t = H - \omega_0 I_0 - \omega_1 I_1$

$$\left.\begin{aligned} H_I &= -\omega_0 I_0 - \omega_1 I_1 + m_e c^2 \gamma + \sqrt{\frac{2(I_0+I_1)\Omega_{ce}}{m_e c^2}}\,\frac{e}{\gamma}\sum_{i=0,1}\frac{B_{w,i}}{k_i}\sin\varphi_i, \\ \gamma &= \sqrt{1 + \frac{(P + k_0 I_0 + k_1 I_1)^2}{m_e^2 c^2} + \frac{2(I_0+I_1)\Omega_{ce}}{m_e c^2}}. \end{aligned}\right\} \tag{2.5}$$

Hamiltonian H_I describes a conservative system ($H_I = \text{const.}$; without loss of generality we take $H_I = 0$) with three degrees of freedom, i.e. with three pairs of conjugate variables (s, P), (φ_0, I_0), (φ_1, I_1). The resonance $\dot{\varphi}_i = 0$ conditions give $I_0 = I_{0R}(s, P, I_1)$, $I_1 = I_{1R}(s, P, I_0)$ as solutions of equations $\omega_i = m_e c^2 \partial\gamma/\partial I_i = 0$. Thus, there are two resonant surfaces. If these surfaces cross (i.e. at the same s, P electron can have simultaneously $I_0 = I_{0R}$ and $I_1 = I_{1R}$), then electrons can simultaneously be in resonance with the two

https://doi.org/10.1017/S0022377821000246 Published online by Cambridge University Press

waves (Zaslavsky *et al.* 2008; Shklyar & Zimbardo 2014). This quite complicated system would require a separate consideration (Lichtenberg & Lieberman 1983; Sagdeev, Usikov & Zaslavsky 1988). Hereafter, we focus instead on the simpler case of well-separated resonances, when resonant surfaces do not cross. Equations $I_0 = I_{0R}$ and $I_1 = I_{1R}$ together with the condition $H_I = 0$ determine two families of curves in (s, P) plane; values I_0 and I_1 are parameters of these families. Thus, on the curve $I_0 = I_{0R}(s, P, I_1)$ there is no change of I_1, and on the curve $I_1 = I_{1R}(s, P, I_0)$ there is no change of I_0. With constant I_1 (or I_0) the I_0 (or I_1) variation is directly related to the variation of energy: $-\omega_0 I_0 - \omega_1 I_1 + m_e c^2 \gamma = 0$. Taking into account that $I_0 + I_1 = I_x = m_e c^2(\gamma^2 - 1)\sin^2\alpha_{\rm eq}/2$, we can plot resonance curves (e.g. Lyons & Williams 1984; Summers *et al.* 1998; Mourenas *et al.* 2012), along which I_i change, in the energy/pitch-angle space $(m_e c^2(\gamma - 1), \alpha_{\rm eq})$ (note that we use the equatorial pitch-angle $\alpha_{\rm eq}$ defined at the minimum of $B_0(s)$ field, i.e. at the minimum of $\Omega_{\rm ce}(s)$). Figure 1(*d*) shows these curves $m_e c^2\gamma - \omega_i I_i = $ const.: each curve of I_0 change corresponds to a fixed value of I_1, and vice versa. Electrons move along these curves with the time step of the interval between resonances. Note between resonances both I_i and γ are conserved, and electrons are moving along adiabatic orbits without wave influence, i.e. energy and pitch-angle change only at the resonances.

Let us consider electron dynamics in the energy/pitch-angle space for the system with Hamiltonian (2.3). We numerically integrate Hamiltonian equations for systems with a single wave and with two waves. Figure 2(*a*,*b*) show electron motion in the energy/pitch-angle space due to the resonance with a single wave. Solid curves are resonant curves of $-\omega_0 I_0 - \omega_1 I_1 + m_e c^2\gamma = $ const. for the wave frequency ω_0 and for the wave frequency ω_1. Electrons move along this curve due to phase bunching (small negative jumps of energy and pitch-angle; see panels (*d*,*e*)) and phase trapping (rare large positive jumps of energy and pitch-angle; see panels (*d*,*e*)). Conservation of $-\omega_0 I_0 - \omega_1 I_1 + m_e c^2\gamma$ and one of the momenta (I_0 or I_1) makes electron dynamics 1-D in the energy/pitch-angle space. However, this dynamics becomes 2-D in the system with two waves, when both I_0 and I_1 change, see figure 2(*c*). The electron moves along resonance curves and jumps between these curves due to I_i jumps. There are still the same energy and pitch-angle jumps due to phase bunching and phase trapping (see panels (*d*,*e*)), but electron phase trajectory covers the entire energy/pitch-angle space. We describe this 2-D dynamics with the mapping technique in this study.

2.2. *Oblique whistler-mode wave*

The second example corresponds to electron resonant interaction with a single oblique ($\theta \neq 0$) wave, for which Hamiltonian (2.1) takes the form

$$\left.\begin{aligned} H &= m_e c^2\gamma + \frac{eB_w}{k\gamma} h_0 \sin(\phi) + \sqrt{\frac{2I_x\Omega_{\rm ce}}{m_e c^2}} h_1 \frac{eB_w}{k\gamma}\sin(\phi + \psi), \\ h_0 &= -\sqrt{\frac{2I_x\Omega_{\rm ce}}{m_e c^2}} C_1 J_1 + \left(\frac{p_\parallel}{m_e c} + C_2\right) J_0 \sin\theta, \\ h_1 &= \frac{1}{2}(J_2(\cos\theta + C_1) + J_0(\cos\theta - C_1)) + \left(\frac{p_\parallel}{m_e c} + C_2\right)\frac{kc}{2\Omega_{\rm ce}}(J_2 + J_0)\sin\theta, \end{aligned}\right\}, \tag{2.6}$$

where we restrict our consideration to the first two resonances: Landau resonance $n = 0$ and the first cyclotron resonance $n = 1$. The Bessel function argument is $\sqrt{2I_x k^2/m_e\Omega_{\rm ce}}\sin\theta$. Such oblique whistler-mode waves are widely observed in the

https://doi.org/10.1017/S0022377821000246 Published online by Cambridge University Press

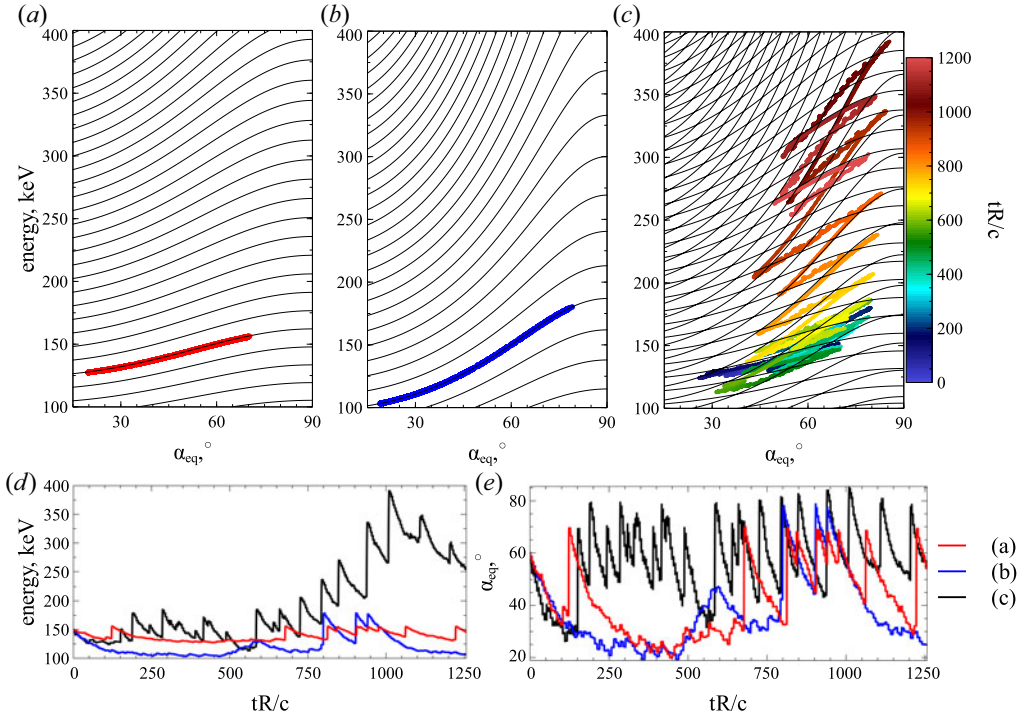


FIGURE 2. Panels (*a–c*) show resonance curves (black) and electron trajectories in the energy/pitch-angle space for Hamiltonian (2.3): only the first whistler-mode wave (*a*), only the second whistler-mode wave (*b*), both whistler-mode waves (*c*). In panel (*c*) different colours correspond to different time intervals. Panels (*d*,*e*) show energy and pitch-angle time series for the three trajectories in panels (*a–c*). We use parameters of dipole field at a radial distance of ~ 5 Earth radii. Plasma density is given by the model from Sheeley *et al.* (2001) and constant along magnetic field lines. Wave frequencies are $\omega_0 = 0.4\Omega_{ce}$, $\omega_1 = 0.2\Omega_{ce}$. Both wave amplitudes are 300 pT (see discussion of such wave observations in Zhang *et al.* (2018) and *Tyler19*). Wave amplitude is distributed along magnetic field lines as $\tanh((\lambda/\delta\lambda_1)^2)\exp(-(\lambda/\delta\lambda_2)^2)$ with λ the magnetic latitude ($ds = Rd\lambda\sqrt{1+\sin^2\lambda}\cos\lambda$) and $\delta\lambda_1 = 2^\circ$, $\delta\lambda_2 = 20^\circ$. This function fits the observed whistler-mode wave intensity distribution (Agapitov *et al.* 2013).

radiation belts (Agapitov *et al.* 2013, 2015*a*; Li *et al.* 2016), and their amplitudes are often sufficiently high for nonlinear resonances (Agapitov *et al.* 2015*b*; Artemyev *et al.* 2016*a*; Mourenas *et al.* 2016*a*). Figure 3 shows an example of an oblique whistler-mode wave measured by THEMIS spacecraft in the outer radiation belt. Electric and magnetic field spectra show the one wave power maximum around $f/f_{ce} \sim 1/3$ (see panels (*a*,*b*)), i.e. this is a single wave. Wave-normal angle $\theta \approx 70^\circ$ (see panel (*c*)), i.e. this wave propagates obliquely to the background magnetic field.

Using the same approach as the one we applied for Hamiltonian (2.3), we introduce wave phases as new variables, $\varphi_0 = \phi_0$ and $\varphi_1 = \phi_1 + \psi$, using the generating function (Neishtadt & Vasiliev 2006; Neishtadt 2014)

$$W = sP + \left(\int k(\tilde{s})\,\mathrm{d}\tilde{s} - \omega t\right) I_0 + \left(\int k(\tilde{s})\,\mathrm{d}\tilde{s} - \omega t + \psi\right) I_1. \tag{2.7}$$

https://doi.org/10.1017/S0022377821000246 Published online by Cambridge University Press

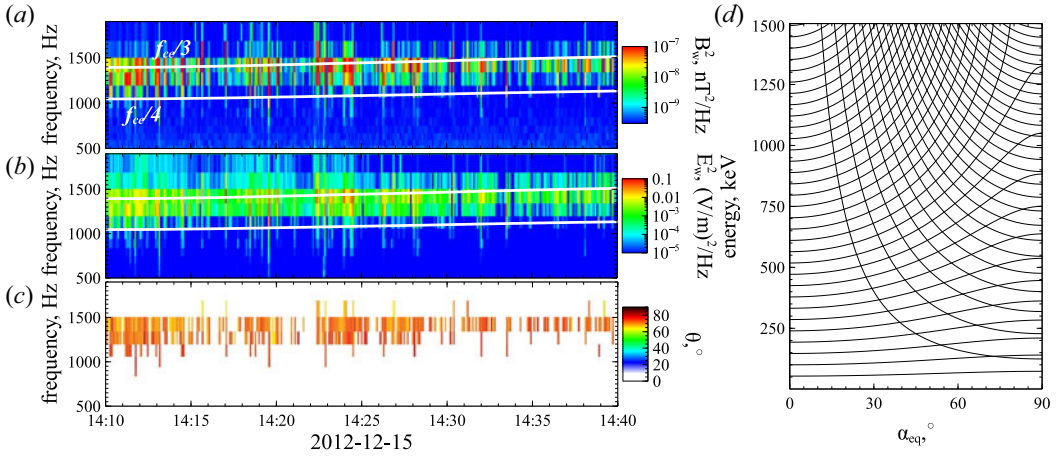


FIGURE 3. Observational example of oblique whistler-mode wave by Van Allen Probe A (Mauk *et al.* 2013): magnetic field spectrum (*a*) and electric field spectrum (*b*) are obtained from EMFISIS measurements (Kletzing *et al.* 2013), wave-normal angle (*c*) is estimated using Mean's method (Means 1972). Resonance curves for the system with two observed whistler-mode waves (*d*).

This function gives the new variables: $P = p - k_0 I_0 - k_1 I_1$, $S = s$ (we keep s notation), $I_x = I_1$ and new Hamiltonian $H_I = H + \partial W/\partial t = H - \omega I_0 - \omega I_1$

$$\left.\begin{aligned} H_I &= -\omega I_0 - \omega I_1 + m_e c^2 \gamma + \frac{eB_w h_0}{k\gamma}\sin\varphi_0 + \sqrt{\frac{2I_1\Omega_{ce}}{m_e c^2}}\frac{eB_w h_1}{k\gamma}\sin\varphi_1, \\ \gamma &= \sqrt{1 + \frac{(P + k_0 I_0 + k_1 I_1)^2}{m_e^2 c^2} + \frac{2I_1\Omega_{ce}}{m_e c^2}}. \end{aligned}\right\} \tag{2.8}$$

The resonance curves in the energy/pitch-angle space are given by two equations: $m_e c^2\gamma - \omega I_1 = \text{const.}$ with $I_1 = I_x = (\gamma^2 - 1)\sin^2\alpha_{eq}/2$ for the cyclotron resonance and $I_x = \text{const.}$ for the Landau resonance. Figure 3(*d*) shows that at $\alpha_{eq} < \pi/4$ Landau resonance curves cross cyclotron resonance curves almost transversely, i.e. in the Landau resonance electrons quickly change energy with weaker pitch-angle change, whereas in the cyclotron resonance the energy change is more effective than the pitch-angle change.

To demonstrate the effects of the two resonances on electron transport in energy/pitch-angle space, we numerically integrate Hamiltonian equations (2.8) for three systems. Figure 4(*a*) shows results of the Landau resonance of the electron and oblique whistler-mode wave. The electron moves along a single resonant curve $I_x = rmconst.$ with phase bunching responsible for pitch-angle increase and energy decrease, and the phase trapping responsible for pitch-angle decrease and energy increase (panels (*d*,*e*)). Figure 4(*b*) shows results of the cyclotron resonance: electron motion in the energy/pitch-angle space are quite similar to motions shown in figure 2(*a*,*b*): phase bunching is responsible for pitch-angle and energy decrease, whereas the phase trapping is responsible for pitch-angle and energy increase (panels (*d*,*e*)). The combination of the two resonances results in rapid electron motion within the whole energy/pitch-angle domain, see figure 4(*c*). The phase bunching decreases electron energy in both resonances, but moves electrons in opposite directions in pitch-angle. As a result, a resonant electron loses energy until it reaches the region with a high probability of trapping into the Landau

https://doi.org/10.1017/S0022377821000246 Published online by Cambridge University Press

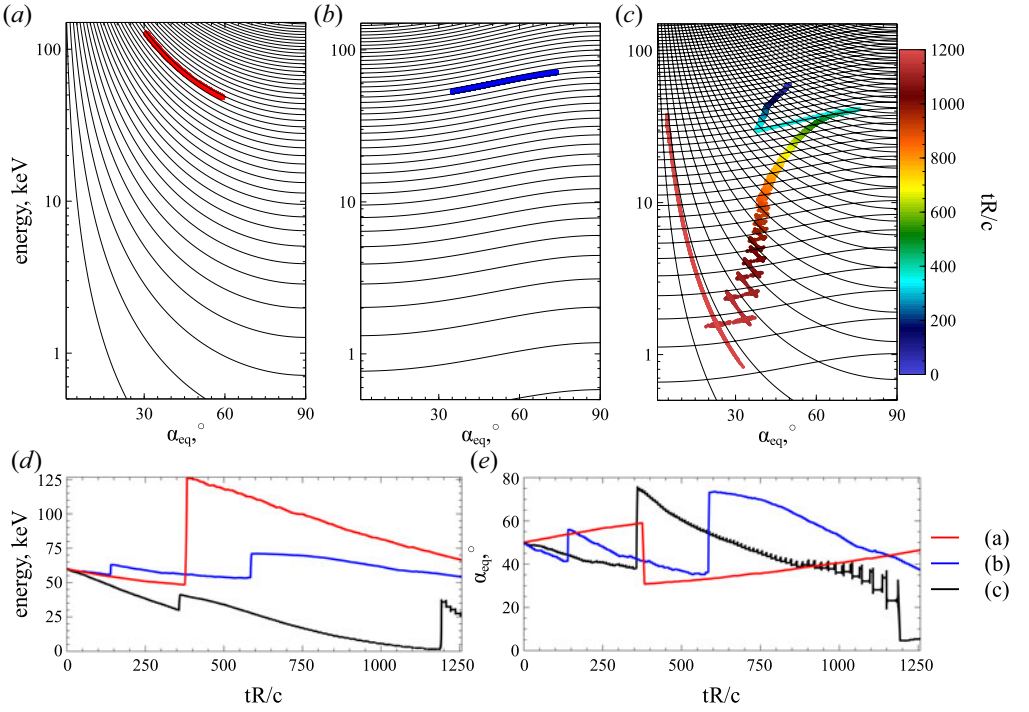


FIGURE 4. Panels (*a–c*) show resonance curves (black) and electron trajectories in the energy/pitch-angle space for Hamiltonian (2.6): only Landau resonance (*a*), only cyclotron resonance (*b*), both resonances (*c*). In panel (*c*) colour shows time. Panels (*d*,*e*) show energy and pitch-angle time series for three trajectories from panels (*a–c*). System parameters are the same as in figure 2, wave frequency is $\omega = 0.35\Omega_{ce}$, wave amplitude is 500 pT and wave-normal angle θ is 5° away of the resonance cone angle $\mathrm{acos}(\omega/\Omega_{ce})$ (see discussion of such wave observations in Wilson *et al.* (2011), Agapitov *et al.* (2014), Artemyev *et al.* (2016*a*) and Mourenas *et al.* (2016*a*)). The wave amplitude distribution along magnetic field-lines is the same as one used in figure 1.

resonance (Artemyev *et al.* 2013). After being trapped in Landau resonance, the electron gains energy and reaches the energy/pitch-angle domain where it can now be trapped into the cyclotron resonance with further energy increase. Such cycles of bunching, Landau trapping and cyclotron trapping, quickly cover a large energy/pitch-angle domain for a single electron trajectory.

2.3. *Field-aligned whistler-mode and EMIC waves*

A third example is a system with field-aligned whistler-mode wave and field-aligned EMIC wave with polarization opposite to the whistler-mode wave. The corresponding Hamiltonian of a relativistic electron (reduction of Hamiltonian (2.2)) takes the form

$$H = m_e c^2 \gamma + \sqrt{\frac{2I_x \Omega_{ce}}{m_e c^2}} \left(\frac{eB_{w,0}}{k_0 \gamma} \sin(\phi_0 + \psi) + \frac{eB_{w,1}}{k_1 \gamma} \sin(\phi_1 - \psi) \right), \tag{2.9}$$

where $k_0 = k_0(\omega_0, s)$ follows the whistler-mode wave dispersion, whereas $k_1 = k_1(\omega_1, s)$ follows the EMIC wave dispersion. Figure 5(*a*,*b*) shows a typical example of observation of such two waves: the high-frequency magnetic field spectrum shows the whistler-mode

https://doi.org/10.1017/S0022377821000246 Published online by Cambridge University Press

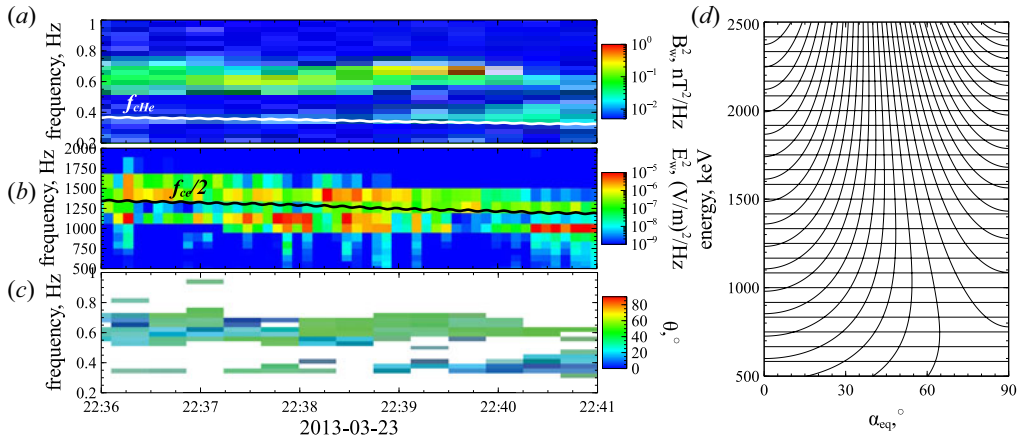


FIGURE 5. Observational example of a system with whistler-mode and EMIC waves by Van Allen Probe A (Mauk *et al.* 2013): magnetic field spectrum of EMIC wave (*a*) and whistler-mode wave (*b*) are obtained from EMFISIS measurements (Kletzing *et al.* 2013), the wave-normal angle of the EMIC wave (*c*) is estimated using Mean's method (Means 1972). Resonance curves for the system with the two observed whistler-mode waves (*d*).

wave with $f/f_{ce} \sim f_{ce}/2$, whereas the low-frequency magnetic field spectrum shows the EMIC wave with $f/f_{cp} \sim f_{cp}/2$ (f_{cp} is the proton gyrofrequency). The EMIC wave is field-aligned (see panel (*c*)). Due to the low EMIC wave frequency, the resonance condition $\dot{\phi}_1 - \dot{\psi} = k_1 p/\gamma - \omega_1 - \Omega_{ce}/\gamma = 0$ can be reduced to $k_1 p = \Omega_{ce}$, with typical k_1 approximately the inverse ion inertial length (Silin *et al.* 2011). Thus, only high-energy electrons (with large enough p) can resonate with EMIC waves (e.g. in the Earth radiation belts the resonant energy is typically larger than ~ 1 MeV, see Thorne & Kennel (1971), Summers & Thorne (2003) and Shprits *et al.* (2016); Chen, Zhu & Zhang (2019)). Let us compare whistler-mode and EMIC wave resonance curves for such high energies.

First, we introduce wave phases as new variables, $\varphi_0 = \phi_0 + \psi$ and $\varphi_1 = \phi_1 - \psi$, with the generating function (Neishtadt & Vasiliev 2006; Neishtadt 2014)

$$W = sP + \left(\int k_0(\tilde{s})\,\mathrm{d}\tilde{s} - \omega_0 t + \psi\right) I_0 + \left(\int k_1(\tilde{s})\,\mathrm{d}\tilde{s} - \omega_1 t - \psi\right) I_1. \tag{2.10}$$

This function gives new variables: $P = p - k_0 I_0 - k_1 I_1$, $S = s$ (we keep s notation), $I_x = I_0 - I_1$ and new Hamiltonian $H_I = H + \partial W/\partial t = H - \omega I_0 - \omega I_1$

$$\left.\begin{aligned} H_I &= -\omega_1 I_0 - \omega_1 I_1 + m_e c^2 \gamma + \sqrt{\frac{2(I_0 - I_1)\Omega_{ce}}{m_e c^2}} \sum_{i=0,1} \frac{eB_{w,i}}{k_i \gamma} \sin\varphi_i, \\ \gamma &= \sqrt{1 + \frac{(P + k_0 I_0 + k_1 I_1)^2}{m_e^2 c^2} + \frac{2(I_0 - I_1)\Omega_{ce}}{m_e c^2}}. \end{aligned}\right\} \tag{2.11}$$

The EMIC resonance curves are given by equation $m_e c^2 \gamma - \omega_1 I_1 = \text{const.}$, and taking into account the smallness of ω_1 we obtain $\gamma \approx 0$, i.e. resonance curves are almost straight lines parallel to the energy axis (see figure 5*d*). The whistler-mode resonance curves ($m_e c^2 \gamma - \omega_0 I_0 = \text{const.}$ with $I_0 = I_x + \text{const.}$) cross these lines: the EMIC wave is responsible for electron transport along pitch-angle space, and the whistler-mode wave

https://doi.org/10.1017/S0022377821000246 Published online by Cambridge University Press

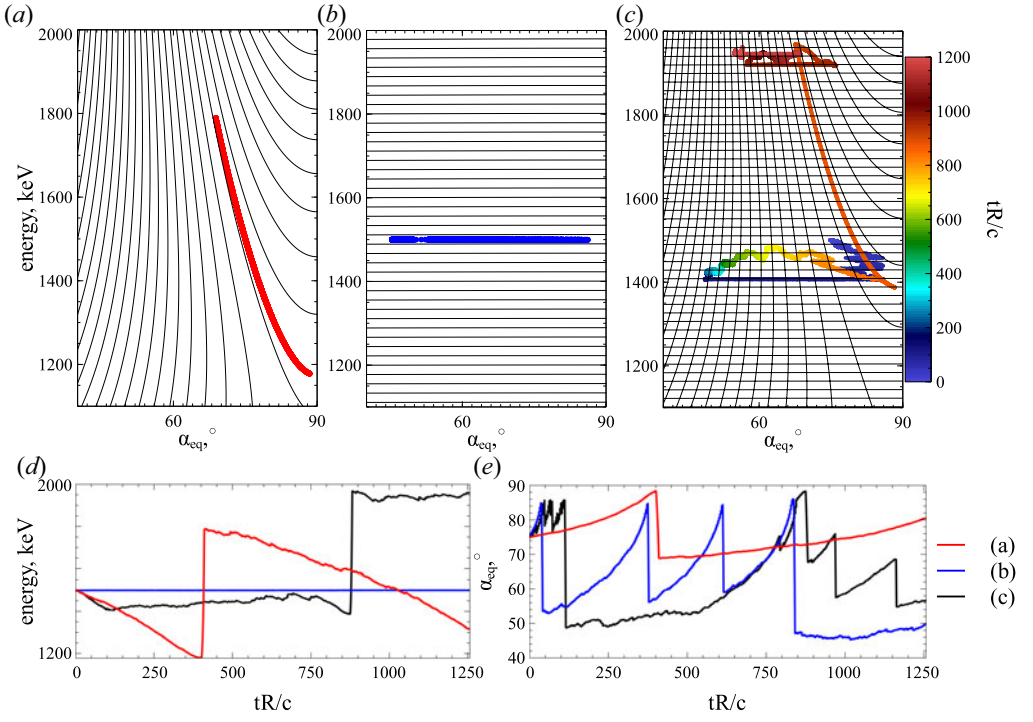


FIGURE 6. Panels (*a–c*) show resonance curves (black) and electron trajectories in the energy/pitch-angle space for Hamiltonian (2.9): only whistler-mode wave (*a*), only EMIC wave (*b*), both whistler-mode and EMIC waves (*c*). In panel (*c*) colour shows time. Panels (*d*,*e*) show energy and pitch-angle time series for three trajectories in panels (*a–c*). System parameters are the same as in figure 2. The EMIC wave is H^+ band with the frequency $\omega = 0.7\Omega_{cp}$ and amplitude 1 nT (see discussion of such wave observations in Kersten *et al.* (2014) and Zhang *et al.* (2016)). Whistler-mode wave frequency is $\omega = 0.35\Omega_{ce}$ and wave amplitude is 300 pT. The wave amplitude distribution along magnetic field-lines is the same as one used in figure 1.

leads to both pitch-angle and energy changes. Figure 6(*a*,*b*) confirms this scenario: the EMIC wave resonates with small pitch-angle (large p) electron and phase bunch it to larger pitch-angles (phase trapping by EMIC waves is responsible for pitch-angle decrease; see panels (*d*,*e*)) with an approximate conservation of energy, whereas the whistler-mode wave can resonate with large pitch-angle electrons and transport them to smaller pitch-angles via phase bunching with energy decrease (moving them away from the EMIC wave resonance).

The combination of EMIC and whistler-mode wave resonances (see figure 6*c*) can result in a very effective transport of large pitch-angle electrons to small pitch-angles (rapid electron losses): bunching of ~ 2 MeV electrons with initially large pitch-angles results in electron transfer to small pitch-angles, where even faster EMIC phase trapping may move this electron to the loss-cone (see discussions of similar effects of combined EMIC and whistler-mode waves in the diffusive approximation in Mourenas *et al.* (2016*b*) and Zhang *et al.* (2017)). From small pitch-angles (note that the loss-cone is not included in our simulations) the EMIC wave can transport an electron via phase bunching to higher pitch-angles, where whistler-mode resonance can accelerate it via trapping. As a result of such different resonant interactions with EMIC and whistler-mode waves, the electron trajectory can quickly fill up a large domain in the energy/pitch-angle space.

https://doi.org/10.1017/S0022377821000246 Published online by Cambridge University Press

3. Mapping technique for multiresonances

To describe the long-term evolution of electron dynamics in the energy/pitch-angle space, we propose to develop a map providing relations for each resonant interaction $\Delta\gamma = \Delta\gamma(\gamma, \alpha_{eq})$, $\Delta\alpha_{eq} = \Delta\alpha(\gamma, \alpha_{eq})$. Changes $\Delta\gamma$, $\Delta\alpha_{eq}$ are due to phase bunching (nonlinear scattering) and phase trapping. Thus, the first step in the construction of such a map is to derive equations for $\Delta\gamma$, $\Delta\alpha_{eq}$ driven by both these processes. We start with Hamiltonian (2.5) and follow the standard procedure of Hamiltonian expansion around the resonant I_0, I_1 values (Neishtadt 2014; Artemyev *et al.* 2018*a*), which are defined by equations $\partial H_I/\partial I_i = 0$,

$$\frac{k_i I_{iR}}{m_e c} = -\frac{P + k_{i'} I_{i'}}{m_e c} - \frac{\Omega_{ce}}{k_i} + \frac{1}{\sqrt{(k_i c/\omega_i)^2 - 1}} \sqrt{1 - \left(\frac{\Omega_{ce}}{k_i c}\right)^2 - 2\frac{\Omega_{ce}}{k_i c}\frac{P + (k_{i'} - k_i) I_{i'}}{m_e c}}, \tag{3.1}$$

where $i' = 0$ for $i = 1$ and $i' = 1$ for $i = 0$. Expansion of Hamiltonian (2.5) around $I_i = I_{iR}$ gives

$$\left.\begin{aligned} H_{Ii} &\approx \Lambda_i + m_e c^2 \tfrac{1}{2} g_i (I_i - I_{iR})^2 + u_{iR} \sin\varphi_i, \\ \Lambda_i &= m_e c^2 \gamma_{iR} - (\omega_0 I_0 + \omega_1 I_1)_{I_i = I_{iR}}, \\ \gamma_{iR} &= \frac{(k_i c/\omega_i)}{\sqrt{(k_i c/\omega_i)^2 - 1}} \sqrt{1 - \left(\frac{\Omega_{ce}}{k_i c}\right)^2 - 2\frac{\Omega_{ce}}{k_i c}\frac{P + (k_{i'} - k_i) I_{i'}}{m_e c}}, \\ u_{iR} &= \sqrt{\frac{2\Omega_{ce}(I_0 + I_1)_{I_i = I_{iR}}}{m_e c^2}}\frac{e}{\gamma_{iR}}\frac{B_{w,i}}{k_i}, \\ g_i &= \left.\frac{\partial^2 \gamma}{\partial I_i^2}\right|_{I_i = I_{iR}} = \frac{k_i^2}{m_e^2 c^2}, \end{aligned}\right\} \tag{3.2}$$

where φ_i are fast variables and $I_i - I_{iR}$) and (s, P) are slow variables (note that Λ_i does not depend on fast variables). Next, we introduce new variables $P_{\varphi i} = I_i - I_{iR}$ with the generating function $Q_i = (I_i - I_{iR})\varphi_i + s\tilde{P}_i$. New Hamiltonians are

$$\begin{aligned} F_i &= \Lambda_i(\tilde{s}, \tilde{P}) + m_e c^2 \tfrac{1}{2} g_i P_{\varphi i}^2 + u_{iR} \sin\varphi_i \\ &\approx \Lambda_i(s, P) + \{\Lambda_i, I_{iR}\}_{s,P}\varphi_i + m_e c^2 t \tfrac{1}{2} g_i P_{\varphi i}^2 + u_{iR} \sin\varphi_i, \end{aligned} \tag{3.3}$$

where $\tilde{s} = s - (\partial I_{iR}/\partial P)\varphi_i$, $\tilde{P} = p + (\partial I_{iR}/\partial s)\varphi_i$, $\{\ \}$ are Poisson brackets, and we expand $\Lambda(\tilde{s}, \tilde{P})$ over small $\partial I_{iR}/\partial s$, $\partial I_{iR}/\partial P$ terms. Hamiltonian F_i is the sum of $\Lambda_i(s, P)$ describing slow variable dynamics and pendulum Hamiltonian describing fast variable dynamics,

$$F_{\varphi i} = m_e c^2 \tfrac{1}{2} g_i P_{\varphi i}^2 + \{\Lambda_i, I_{iR}\}_{s,P}\varphi_i + u_{iR} \sin\varphi_i, \tag{3.4}$$

where the coefficients depend on the slow variables. Figure 7 shows phase portraits of $F_{\varphi i}$ for systems with $a_i = |u_{iR}/\{\Lambda_i, I_{iR}\}| < 1$ (panel (*a*)) and with $a_i = |u_{iR}/\{\Lambda_i, I_{iR}\}| > 1$ (panel (*b*)). For low wave amplitude $a_i < 1$ the phase portrait does not contain closed orbits, i.e. all particles cross the resonance $\dot{\varphi}_i = m_e c^2 g_i P_{\varphi,i} = 0$ within an interval of approximately one period of φ_i. There are only weak scatterings in this regime with zero mean changes of I_i, and such scatterings can be described by the quasi-linear diffusion model for inhomogeneous plasma (e.g. Karpman 1974; Albert 2010; Grach & Demekhov 2020). For sufficiently high wave amplitude $a_i > 1$, however, the phase

https://doi.org/10.1017/S0022377821000246 Published online by Cambridge University Press

portrait contains both closed and open orbits, i.e. there are now phase trapped particles oscillating around the resonance $\dot{\varphi}_i = m_e c^2 g_i P_{\varphi,i} = 0$ for a long time. Scattering (crossing of the resonance along the open orbits) would result in phase bunching with a small, yet non-zero mean change of I_i (see reviews by Shklyar & Matsumoto (2009), Albert *et al.* (2013) and references therein), whereas phase trapping would significantly change I_i. We would like to include this nonlinear regime of wave–particle interaction into the map in energy/pitch-angle space. For this reason, we derive expressions for changes of I_i due to phase bunching, $\Delta_{\rm scat} I_i$, and due to phase trapping $\Delta_{\rm trap} I_i$. As $\Delta_{\rm scat} I_i$ is local, i.e. depends on particle and system characteristics at the resonance, we can keep slow variables unchanged for $\Delta_{\rm scat} I_i$ evaluations

$$\Delta_{\rm scat} I_i = 2\int_{-\infty}^{t_{iR}} \frac{\partial H_{Ii}}{\partial I}\,{\rm d}t = \frac{2u_{iR}}{m_e c^2 g_i}\int_{-\infty}^{\varphi_{iR}} \frac{\cos\varphi_i\,{\rm d}\varphi_i}{P_{\varphi i}}$$

$$= \sqrt{\frac{2u_{iR}}{m_e c^2 g_i}}\int_{-\infty}^{\varphi_{iR}} \frac{\sqrt{u_{iR}}\cos\varphi_i\,{\rm d}\varphi_i}{\sqrt{F_{\varphi i} - \{\Lambda_i, I_{iR}\}_{s,P}\varphi_i - u_{iR}\sin\varphi_i}}$$

$$= \sqrt{\frac{2u_{iR}}{m_e c^2 g_i}}\int_{-\infty}^{\varphi_{iR}} \frac{\sqrt{u_{iR}}\cos\varphi_i\,{\rm d}\varphi_i}{\sqrt{\{\Lambda_i, I_{iR}\}_{s,P}(\varphi_{Ri} - \varphi_i) + u_{iR}(\sin\varphi_{Ri} - \sin\varphi_i)}}$$

$$= \sqrt{\frac{2u_{iR}}{m_e c^2 g_i}}\int_{-\infty}^{\varphi_{iR}} \frac{\sqrt{a_i}\cos\varphi_i\,{\rm d}\varphi_i}{\sqrt{(\varphi_{Ri} - \varphi_i) + a_i(\sin\varphi_{Ri} - \sin\varphi_i)}} = \sqrt{\frac{2u_{iR}}{m_e c^2 g_i}} f_i(\varphi_{Ri}, a_i), \qquad (3.5)$$

where t_{iR} is the time of passage through the resonance, φ_{iR} is the wave phase at this time, and we use $\dot{\varphi}_i = m_e c^2 g_i P_{\varphi i} = 2^{1/2}\sqrt{F_{\varphi i} - \{\Lambda_i, I_{iR}\}\varphi_i - u_{Ri}\sin\varphi_i}$, $F_{\varphi i} = \{\Lambda_i, I_{iR}\}\varphi_{Ri} + u_{Ri}\sin\varphi_{Ri}$ (resonant energy $F_{\varphi i}$ value evaluated at $P_{\varphi i} = 0$). Note (3.5) describes the $\Delta_{\rm scat} I_i$ change for the particle motion throughout the resonance from $-\infty$ to resonant φ_{iR}, whereas the motion in the opposite direction would result in the change of sign of $\Delta_{\rm scat} I_i$. Function $f_i(a_i, \varphi_{iR})$ is periodic for φ_{iR}, see figure 7(*c*). Although the sign of f_i changes within one φ_{iR} period, the mean value of this function for $a_i > 1$ is not zero, providing the effect of phase bunching. To consider the precise $\Delta_{\rm scat} I_i$ dependence on φ_{iR} in the mapping, one would need to keep information about resonant phase φ_i and calculate the phase gain between resonances. However, the phase is fast rotating, and even a small change of φ_i at the resonance would result in a significant change of phase gain between resonances. Therefore, we can assume that φ_{iR} is a random variable with a uniform distribution of the resonant energy $F_{\varphi i}(\varphi_{iR})$ at $P_{\varphi i} = 0$ axis (see justification of this assumption in Itin *et al.* (2000), Artemyev *et al.* (2020*a*) and Artemyev *et al.* (2020*b*)), and all resonant particles with the same slow variables (same energy and pitch-angle) at the resonance would experience the same ΔI_i change equal to $\langle \Delta I_i \rangle$ averaged over the resonant energy (Artemyev *et al.* 2020*b*).

An important property of the f function from (3.5) is that being averaged over energies in resonance, $F_{\varphi i} = \{\Lambda_i, I_{iR}\}\varphi_{Ri} + u_{Ri}\sin\varphi_{Ri}$, this function gives

$$\langle f_i \rangle = -\sqrt{\frac{m_e c^2 g_i}{2u_{iR}}}\frac{S}{2\pi} = -\sqrt{\frac{8|u_{iR}|}{a_i m_e c^2 g_i}}\int_{\varphi_{i-}}^{\varphi_{iR}} \sqrt{(\varphi_{Ri} - \varphi_i) + a_i(\sin\varphi_{Ri} - \sin\varphi_i)}\,{\rm d}\varphi_i, \quad (3.6)$$

where S is the area surrounded by the separatrix in the phase portrait in figure 7(*b*) (see details of (3.6) derivations in Neishtadt (1999) and Artemyev *et al.* (2018*a*)). Therefore, the $\Delta_{\rm scat} I_i$ change due to phase bunching is equal to $-S/2\pi$ and for $a_i \gg 1$

https://doi.org/10.1017/S0022377821000246 Published online by Cambridge University Press

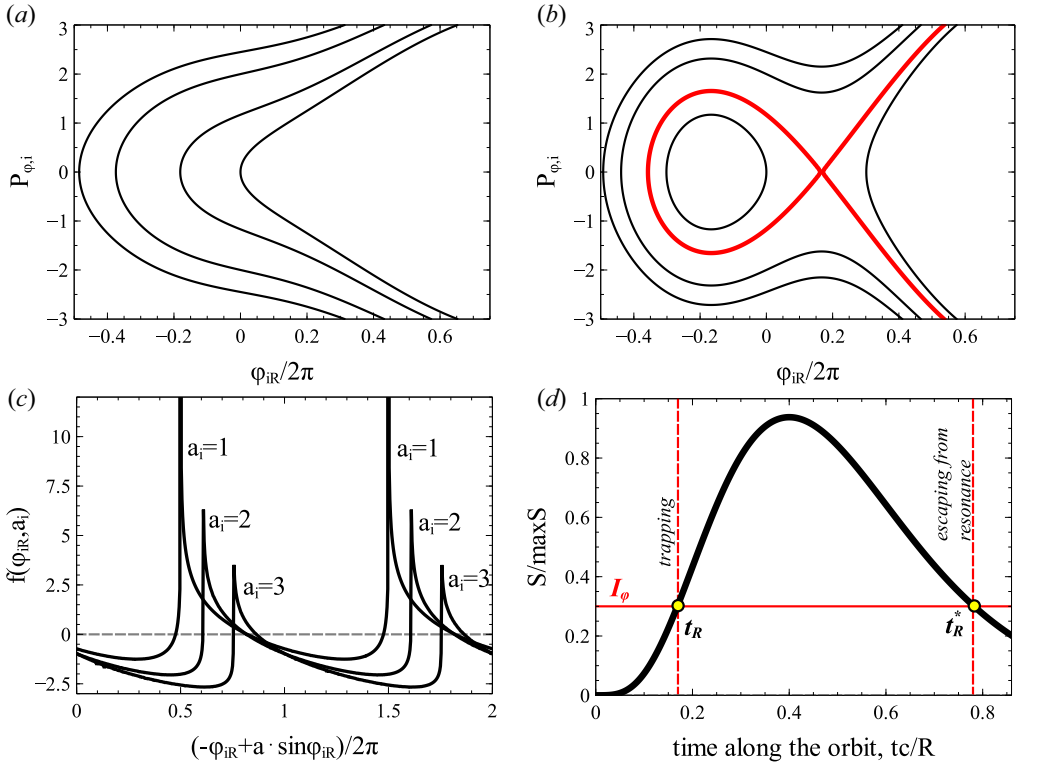


FIGURE 7. Phase portraits of $F_{\varphi i}$ for systems with $|u_{iR}| < |\{\Lambda_i, I_{iR}\}|$ (a) and with $|u_{iR}| > |\{\Lambda_i, I_{iR}\}|$ (b). Black curves show contours of $F_{\varphi,i} = \text{const.}$, red curve is the separatrix demarcating region of trapped (closed) electrons orbits and region of transient (open) orbits. Function $f(h_\phi, a)$ for several a and $(-\varphi_{iR} + a\sin\varphi_{iR})/2\pi$ (c) and scheme of trapping/detrapping (d).

(i.e. for very weak magnetic field inhomogeneity; note $\{\Lambda_i, I_{iR}\} \sim \partial/\partial s$) we have $\Delta_{\text{scat}} I_i = -8\sqrt{2u_{iR}/m_e c^2 g_i}$ where $S = 16\sqrt{2u_{iR}/m_e c^2 g_i}$ is the width of the resonance for large amplitude waves (Palmadesso 1972; Karimabadi *et al.* 1990).

The change of I_i due to phase bunching (nonlinear scattering) is sufficiently small to consider this process locally in energy/pitch-angle space, i.e. $\Delta_{\text{scat}} I_i \ll I_i$ (see discussion of exceptions for $\Delta_{\text{scat}} I_i \sim I_i$ in Appendix A), whereas the change of I_i due to phase trapping is essentially non-local. To evaluate $\Delta_{\text{trap}} I_i$, we take into account that $I_i = I_{iR}$ in the resonance (during the trapping), the trapping time is defined as $2\pi I_\phi = \int P_{\varphi i}\, \mathrm{d}\varphi_{iR} = S$, and I_ϕ is conserved during the trapping (because trapped particles oscillate in the $(\varphi_{iR}, P_{\phi i})$ plane much faster than the system evolves (much faster than variations of slow variables s, P). Thus, the trapping time is defined as the time of arrival to the resonance t_R with $\dot{S}(t_R) > 0$ (the growth of the area surrounded by the separatrix allows trapping of particles moving along open trajectories into closed trajectories), whereas the time t_R^* of escape from the trapping is defined by $S(t_R^*) = S(t_R)$ and $\dot{S}(t_R^*) < 0$ (see scheme in figure 7*d*)

$$\Delta_{\text{trap}} I_i = I_{iR}(t_{iR}^*) - I_{iR}(t_{iR}), \quad S(t_{iR}^*) = S(t_{iR}), \quad \dot{S}(t_{iR}) > 0, \quad \dot{S}(t_{iR}^*) < 0. \qquad (3.7a\text{–}d)$$

At the resonance, an electron can be scattered (i.e. experience the phase bunching) or trapped, and this depends on the φ_{iR} value (e.g. Albert 1993; Itin *et al.* 2000;

https://doi.org/10.1017/S0022377821000246 Published online by Cambridge University Press

Grach & Demekhov 2018). However, as φ_{iR} is a fast oscillating variable, we can consider the so-called probability of trapping instead of tracing the precise φ_{iR} value: the range of φ_{iR} of trapped particles, i.e. the ratio of trapped particles to the total number of resonant particles for a single resonance, is the probability of trapping, Π_i (e.g. Arnold, Kozlov & Neishtadt (2006), and references therein). For small Π_i, this probability is defined as the ratio of the change of the area under the separatrix, $\dot{S}$, and the total resonant flux $\int_0^{2\pi} \dot{P}_{\varphi,i}\,\mathrm{d}\phi = 2\pi\{\Lambda_i, I_{iR}\}$: $\Pi_i = \dot{S}/2\pi\{\Lambda_i, I_{iR}\} = \{S, F_i\}/2\pi\{\Lambda_i, I_{iR}\}$. This definition of the trapping probability has been verified for various plasma systems (e.g. Artemyev *et al.* 2014*a*; Leoncini, Vasiliev & Artemyev 2018; Vainchtein *et al.* 2018). Therefore, the resonant interaction can be characterized by Π, $\Delta_{\mathrm{trap}} I_i$ and $\Delta_{\mathrm{scat}} I_i$.

Due to conservation of $H_i = m_e c^2 \gamma - \omega_0 I_0 - \omega_1 I_1$, changes of I_i are directly related to γ changes, whereas the $I_x = I_0 + I_1$ relation gives the pitch-angle change

$$\frac{\omega_i \sin^2\alpha_{\mathrm{eq}}}{\gamma^2-1}(\Delta_i\gamma)^2 - 2\Delta_i\gamma\frac{\Omega_{\mathrm{eq}} - \gamma\omega_i\sin^2\alpha_{\mathrm{eq}}}{\gamma^2-1} + \omega_i(\sin^2(\alpha_{\mathrm{eq}} + \Delta_i\alpha_{\mathrm{eq}}) - \sin^2\alpha_{\mathrm{eq}}) = 0, \tag{3.8}$$

that for small changes (phase bunching) can be rewritten as

$$\Delta_i\alpha_{\mathrm{eq}} = \Delta_i\gamma\frac{\Omega_{\mathrm{eq}} - \gamma\omega_i\sin^2\alpha_{\mathrm{eq}}}{\omega_i\sin\alpha_{\mathrm{eq}}\cos\alpha_{\mathrm{eq}}(\gamma^2-1)}. \tag{3.9}$$

Therefore, the map for one resonance can be written as

$$\left.\begin{aligned}
\begin{pmatrix}\bar{\gamma}\\ \bar{\alpha}_{\mathrm{eq}},\end{pmatrix} &= \begin{pmatrix}G_{\gamma i}(\gamma,\alpha_{\mathrm{eq}})\\ G_{\alpha i}(\gamma,\alpha_{\mathrm{eq}})\end{pmatrix} = \begin{pmatrix}\gamma\\ \alpha_{\mathrm{eq}}\end{pmatrix} + \begin{pmatrix}\Delta_i\gamma\\ \Delta_i\alpha_{\mathrm{eq}}\end{pmatrix},\\
\Delta_i\gamma &= \omega_i\begin{cases}\Delta_{\mathrm{scat}} I_i(\gamma,\alpha_{\mathrm{eq}}), & \xi_i \in [\Pi_i(\gamma,\alpha_{\mathrm{eq}}), 1]\\ \Delta_{\mathrm{trap}} I_i(\gamma,\alpha_{\mathrm{eq}}), & \xi_i \in [0, \Pi_i(\gamma,\alpha_{\mathrm{eq}})]\end{cases}\\
\Delta_i\alpha_{\mathrm{eq}} &= \begin{cases}\dfrac{\Omega_{\mathrm{eq}} - \gamma\omega_i\sin^2\alpha_{\mathrm{eq}}}{\sin\alpha_{\mathrm{eq}}\cos\alpha_{\mathrm{eq}}(\gamma^2-1)}\Delta_{\mathrm{scat}} I_i(\gamma,\alpha_{\mathrm{eq}}), & \xi_i \in [\Pi_i(\gamma,\alpha_{\mathrm{eq}}), 1]\\ \Delta_i\alpha_{\mathrm{eq}}(\Delta_{\mathrm{trap}} I_i, \gamma, \alpha_{\mathrm{eq}}), & \xi_i \in [0, \Pi_i(\gamma,\alpha_{\mathrm{eq}}))\end{cases}
\end{aligned}\right\} \tag{3.10}$$

where ξ_i is a random variable uniformly distributed in [0, 1]. If there are two resonances (one with the first wave and another one with the second wave) during one electron bounce period τ_b, then over this period the electron energy/pitch-angle change should be

$$\begin{pmatrix}\bar{\gamma}\\ \bar{\alpha}_{\mathrm{eq}}\end{pmatrix} = \begin{pmatrix}G_{\gamma 1}(G_{\gamma 0}(\gamma,\alpha_{\mathrm{eq}}), G_{\alpha 0}(\gamma,\alpha_{\mathrm{eq}}))\\ G_{\alpha 1}(G_{\gamma 0}(\gamma,\alpha_{\mathrm{eq}}), G_{\alpha 0}(\gamma,\alpha_{\mathrm{eq}}))\end{pmatrix}. \tag{3.11}$$

Figure 8 shows 10 main characteristics of map (3.11) in the energy/pitch-angle space: amplitudes of scattering $\Delta_{scat,i}\gamma$, $\Delta_{scat,i}\alpha_{\mathrm{eq}}$; amplitudes of trapping $\Delta_{trap,i}\gamma$, $\Delta_{trap,i}\alpha_{\mathrm{eq}}$; and trapping probabilities Π_i for two field-aligned whistler-mode waves. To derive these characteristics for given energy and pitch-angle, we (1) calculate $\gamma, \alpha_{\mathrm{eq}}$ and resonance location s_R given by equation $I_i = I_{iR}$; (2) determine coefficients of Hamiltonian $F_i, S, \dot{S}$, and trapping probability Π at s_R; (3) determine $\Delta_{\mathrm{scat}} I_i = -S/2\pi$, position of escape from the resonance s_R^* (if $\dot{S}(s_R) > 0$), and $\Delta_{\mathrm{trap}} I_i = I_{iR}(s_R^*) - I_{iR}(s_R)$; (4) recalculate $\Delta_{\mathrm{scat}} I_i$, $\Delta_{\mathrm{trap}} I_i$ into energy and pitch-angle changes. Numerical verification

https://doi.org/10.1017/S0022377821000246 Published online by Cambridge University Press

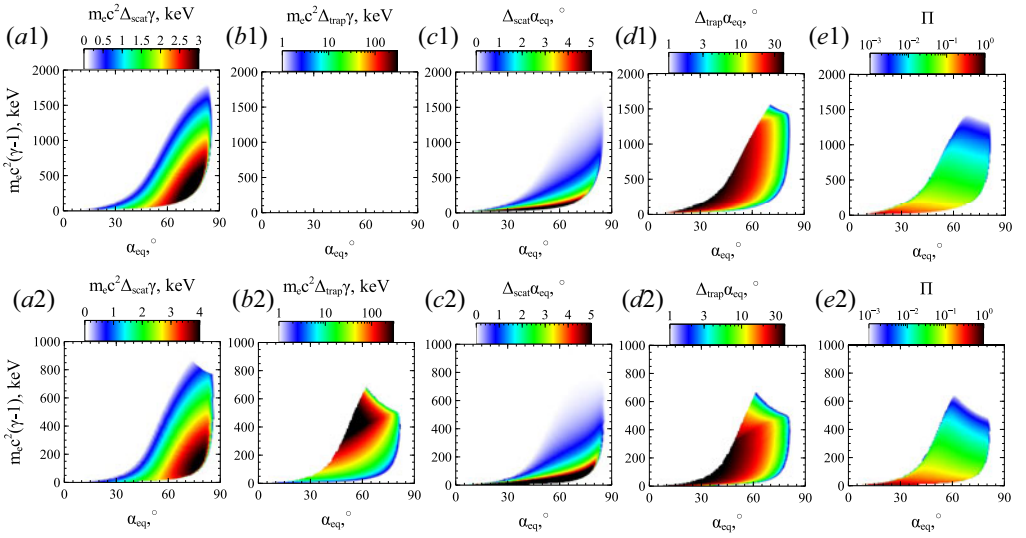


FIGURE 8. System characteristics for two field-aligned whistler-mode waves with the parameters as in figure 1: energy change due to scattering (*a*) and trapping (*b*), pitch-angle change due to scattering (*c*) and trapping (*d*), trapping probability (*e*).

of this technique of $\Delta_{scat,i}\gamma$, $\Delta_{trap,i}\gamma$, Π_i with test particle trajectories can be found in Vainchtein *et al.* (2018) and Artemyev *et al.* (2020*b*).

Substituting characteristics from figure 8 into map (3.11), we evaluate dynamics of resonant electrons. Figure 9 shows a sample trajectory: energy and pitch-angle are plotted versus the number of iterations k and versus time $t = \sum_k \tau_{b,k}(\gamma, \alpha_{\rm eq})$. The trajectory obtained with the mapping technique contains all elements that can be found in the numerically integrated trajectory (compare with figure 2): energy decrease due to phase bunching and rare jumps due to phase trapping. Note that the bounce period is given by $\tau_b = 4\int_0^{s_{\max}} {\rm d}s/p$ with $p = m_e c^2\sqrt{1-\gamma-2I_x\Omega_{\rm ce}(s)}$ and $2I_x\Omega_{\rm ce}(s_{\max}) = 1-\gamma$. Any direct comparison of trajectories obtained via numerical integration and mapping technique is not possible due to significant randomization of resonant electron motion, i.e. trajectories in energy/pitch-angle plane for two test electrons can differ significantly even with small difference of initial electron phases (e.g. Shklyar 1981; Le Queau & Roux 1987; Albert 2001). Thus, the verification of map (3.11) is mainly based on verification of (3.5) and (3.7*a–d*) (see Artemyev *et al.* 2015, 2016*b*; Vainchtein *et al.* 2018) and on verification of 1D analogues of this map (see Artemyev *et al.* 2020*b*).

Using map (3.11), we can simulate the evolution of the electron distribution function as an ensemble of test trajectories. We start with the test simulation of electron spread in the energy/pitch-angle space. Four populations of electrons with small ranges of initial energy and pitch-angles are traced for 500 interactions and their positions in energy/pitch-angle space are shown at six different times, see figure 10. White colour shows the area of resonant wave–particle interaction (see Appendix B for a definition of this area and for technical details of the map (3.11) application). Electrons of different initial populations quickly (already after $tc/R \sim 50$, i.e. ∼15 resonant interactions) spread within a wide pitch-angle range, but are somehow separated in energy. After $tc/R \sim 300$ (∼80 resonant interactions) the populations fill large areas in energy/pitch-angle space and start overlapping. After $tc/R \sim 1000$ (∼250 resonant interactions) the entire energy/pitch-angle space is covered, and electrons from low energy populations (black and blue) reach high

https://doi.org/10.1017/S0022377821000246 Published online by Cambridge University Press

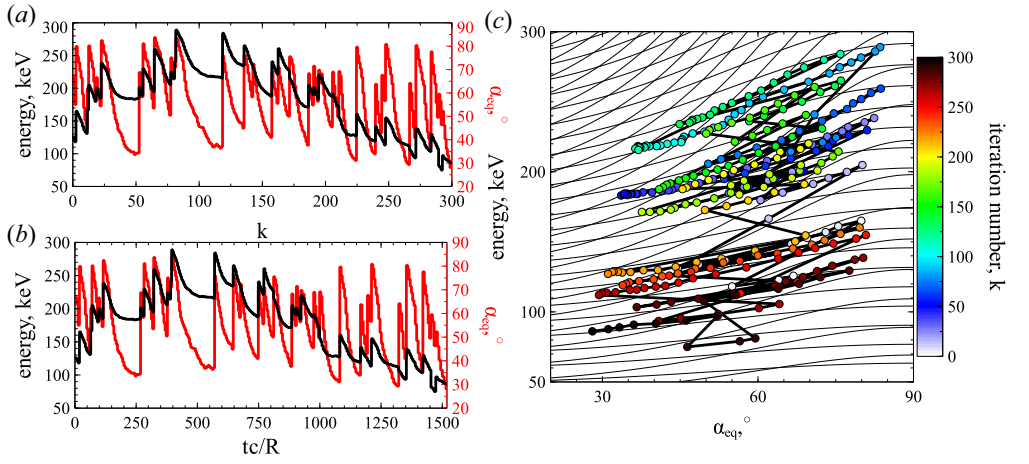


FIGURE 9. A sample trajectory obtained using map (3.11): energy and pitch-angle versus number of map iterations (*a*), energy and pitch-angle versus time (*b*), particle trajectory in the energy/pitch-angle space (*c*).

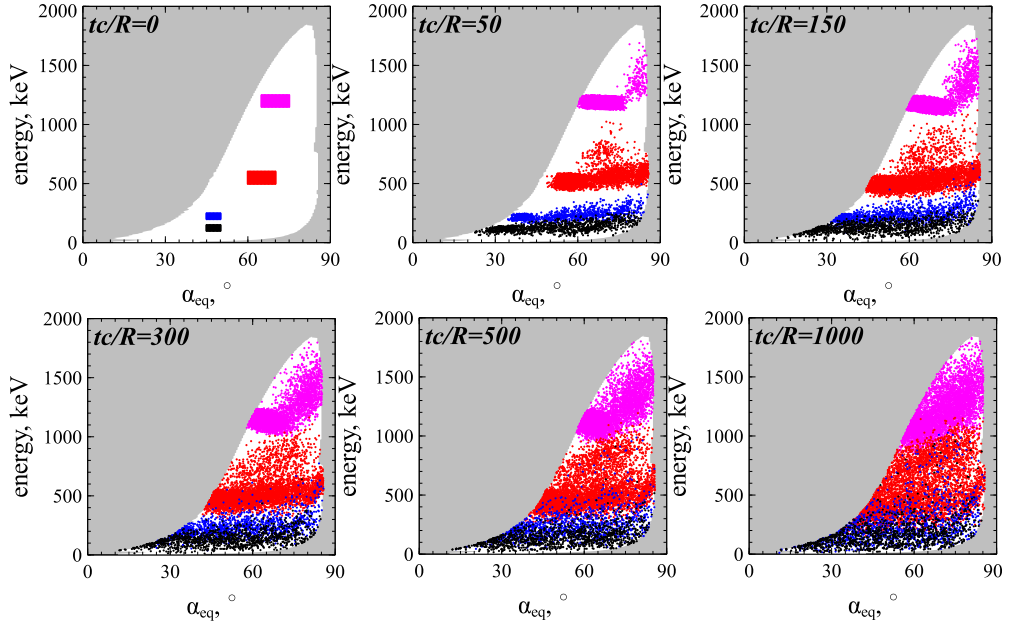


FIGURE 10. Evolution of four electron populations modelled with map (3.11). Six moments of time are shown. White colour shows the area of wave–particle nonlinear resonant interaction, see Appendix B.

energies (∼1 MeV), whereas electrons from high-energy populations (red and magenta) decelerate with energy losses of several hundred keVs. Such fast phase mixing should result in spreading and smoothing of the electron phase space density.

To examine the evolution of the electron phase space density, we start with a power law distribution $f_0(\gamma, \alpha) = C \cdot \sin\alpha_{eq} \cdot (\gamma - 1)^{-3}$ typical in the radiation belts, and fit this distribution by 2×10^7 trajectories. There are 180×400 pitch-angle/energy values,

https://doi.org/10.1017/S0022377821000246 Published online by Cambridge University Press

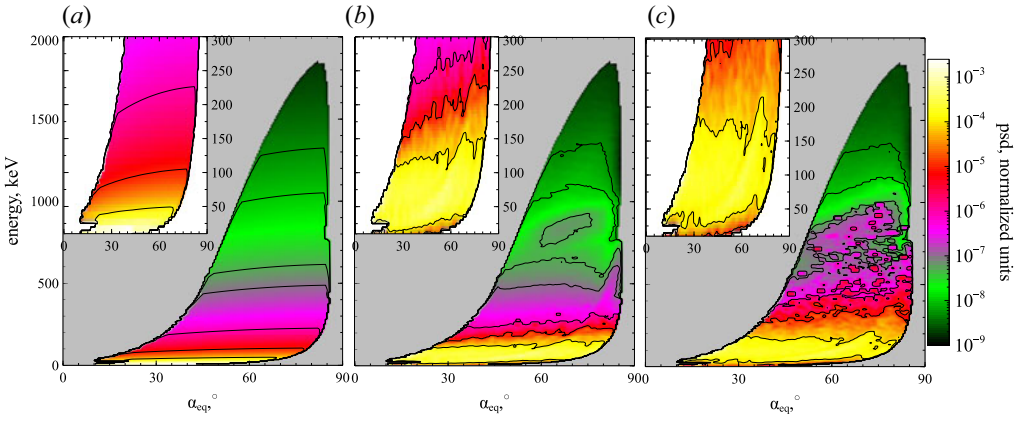


FIGURE 11. Evolution of electron distribution modelled with map (3.11). Three moments of time are shown: $tc/R = 0$ (a), $tc/R = 300$ (b), $tc/R = 1000$ (c). The initial distribution $f_0(\gamma, \alpha) = C \cdot \sin\alpha_{eq} \cdot (\gamma - 1)^{-3}$ in panel (a).

and ~ 22600 within the resonant area; for each value within the resonant area, we run 1000 trajectories. Each trajectory is traced for 300 interactions with the map (3.11), and corresponding $\alpha_{eq}(k)$, $\gamma(k)$ profiles transferred to time series. Then, we recalculate the distribution from f_0 using phase space density conservation along the trajectories. Figure 11 shows three snapshots of the distribution $f(\alpha, \gamma)$ at different times (inserted panels show the low energy subinterval). The rapid evolution of the distribution function results in phase space density flattening within the resonant region: there is an increase of high-energy/small pitch-angle phase space density and a decrease of low energy/large pitch-angle phase space density. During the simulation time, one electron can be trapped several times, i.e. most of particles circulate in the energy/pitch-angle space, because trappings bring them to the high energy region from which they then drift by bunching. Such a circulation also comprises successive trappings by two waves that bring electrons to the very high-energy region, whereas long periods of phase bunching without trappings can transport very energetic electrons to quite low energies. The last two phenomena are less frequent, and mixing of $\sim$1 MeV electrons with $<$100 keV electrons is slower than mixing within energy localized domains.

The general trend of the resonant electron transport in the energy/pitch-angle space is the reduction of phase space density gradients. In the presence of a single wave, such a gradient smoothing occurs along the resonant curves, $\gamma - \omega_0 I_0 = \text{const}$. (Artemyev *et al.* 2020*b*). In systems with two waves, the intersection of resonant curves $\gamma - \omega_0 I_0 = \text{const}$. and $\gamma - \omega_1 I_1 = \text{const}$. results in 2-D gradient smoothing, i.e. we can expect a reduction of gradients in energy space after integration over pitch-angle. Figure 12 shows such electron acceleration: increase of high-energy population and decrease of low energy population that result in gradient smoothing. This is the typical evolution of the electron distribution due to resonant interaction with whistler-mode waves (see similar results for nonlinear (Vainchtein *et al.* 2018) and quasi-linear (Thorne *et al.* 2013; Li *et al.* 2014) simulations).

4. Discussion and conclusions

The proposed approach allows us to investigate the long-term evolution of the electron distribution function in a system with nonlinear wave–particle interaction. This approach is based on the mapping technique that significantly simplifies electron trajectory integration

https://doi.org/10.1017/S0022377821000246 Published online by Cambridge University Press

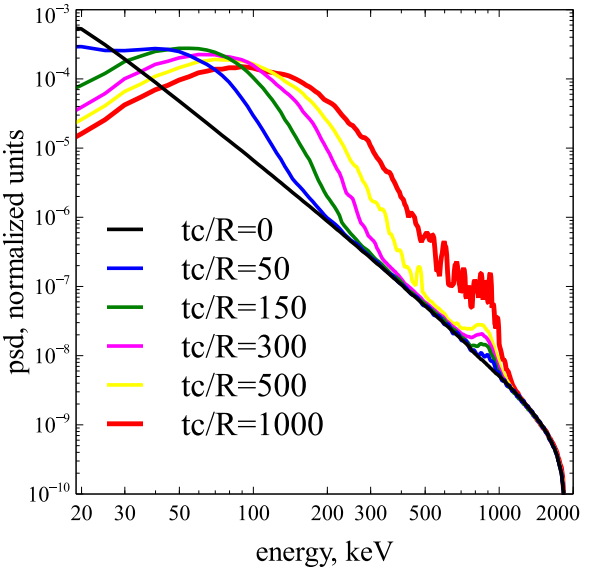


FIGURE 12. Pitch-angle integrated electron distribution, $\int_0^{\pi} \sin\alpha_{eq} \cdot psd(E, \alpha_{eq})\, d\alpha_{eq}$, from figure 11.

by excluding from the consideration the main, adiabatic part of electron orbits and by focusing only on small intervals of resonant electron phase bunching and trapping. This approach is somewhat analogous to the Green function method proposed by Furuya *et al.* (2008) and Omura *et al.* (2015), and to the nonlinear kinetic equation proposed by Artemyev *et al.* (2016*b*) and Vainchtein *et al.* (2018). However, contrary to these other methods, the mapping does not require a very fine discretization of energy/pitch-angle space and it can easily be generalized to multiwave systems. Resonances with different waves are very important for the destruction of the symmetry typical for the single wave system, where conservation of $(\gamma - \omega I)$ results in a reduced mixing in energy/pitch-angle space. Already, two waves with different characteristics are sufficient to produce a total mixing in energy/pitch-angle space (see figure 10) and a smoothing (reduction) of electron phase space density gradients (see figure 12). The similar effect of fast mixing due to two independent resonances has been found in various dynamical systems with quite general properties (e.g. Gelfreich *et al.* 2011; Itin & Neishtadt 2012).

Moreover, note that our simulations shown in figures 9–12 are quite localized in time, since $R/c \sim 1000$ is approximately 100 s in the outer radiation belt ($L \sim 5$), and that this time period is much smaller than the characteristic time of evolution of any process typically modelled by quasi-linear theory (Thorne *et al.* 2013; Drozdov *et al.* 2015; Albert *et al.* 2016; Ma *et al.* 2016, 2018). Therefore, we extend the simulation interval to $tc/R = 2.5 \times 10^4$ (∼40 min) to show that this time scale is already sufficiently long to almost fully smooth gradients within <1 MeV, see figure 13. Generally, however, 40 minutes is a too long interval to keep whistler-mode wave activity at the same high level (although such long-living regions of intense waves are sometimes observed, see Cully, Bonnell & Ergun (2008), Agapitov *et al.* (2015*b*) and Cattell *et al.* (2015)).

Figure 8 shows energy/pitch-angle domains of nonlinear wave–particle interaction, and these domains are used for the simulation of the electron distribution function evolution (see figures 10–13 and Appendix B). For simplicity, we assume that the boundary of these domains is impenetrable. However, additionally to nonlinear wave–particle interactions

https://doi.org/10.1017/S0022377821000246 Published online by Cambridge University Press

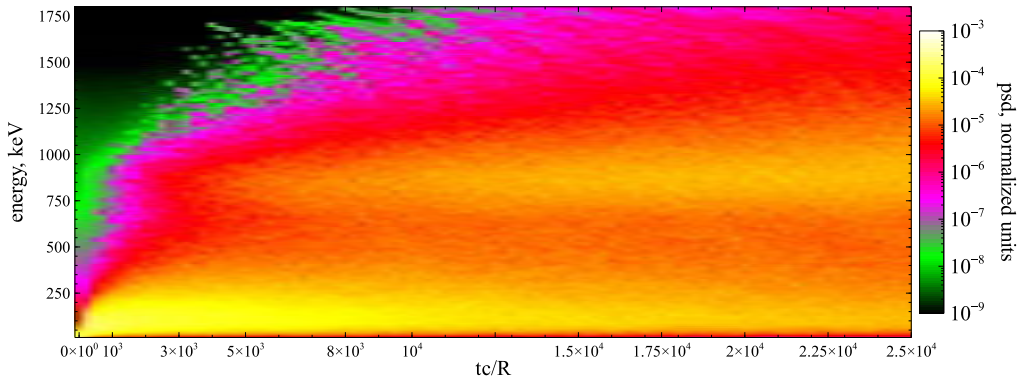


FIGURE 13. Evolution of pitch-angle integrated electron distribution, $\int_0^{\pi} \sin\alpha_{eq} \cdot psd(E, \alpha_{eq})\, d\alpha_{eq}$ in a long-term simulation (*psd* is the electron phase space density).

(phase bunching and phase trapping), there is also in reality some electron diffusion. This diffusion is finite everywhere in the energy/pitch-angle plane where there is an electron resonance with the whistler-mode wave. Thus, this diffusion would transport electrons across the boundary of the domains of nonlinear wave–particle interaction. The direction of this transport depends on the phase space density gradients. At low energies, the nonlinear wave–particle interaction results in phase space density decrease (see figure 13), and thus pitch-angle diffusion will bring new small-energy particles into these domains. At high energies, the nonlinear wave–particle interaction results in phase space density increase (see figure 13), and thus both energy and pitch-angle diffusion will try to spread this phase space density maximum. Such diffusion can be included into the map (3.11) as random energy and pitch-angle jumps with zero mean values and amplitudes given by the quasi-linear model (e.g. Albert 2010). However, the diffusion is generally much weaker than nonlinear phase bunching and trapping, and the diffusion-driven evolution of the phase space density should mostly appear after nonlinear wave–particle interaction has already partly smoothed the initial phase space density gradients (Artemyev *et al.* 2019*a*).

The map (3.11) has been constructed for electron interaction with monochromatic waves (see (2.1)), whereas spacecraft observations in the Earth's radiation belts often report about more complex wave field distributions, e.g. significant wave amplitude modulation (Tao *et al.* 2013; Santolık *et al.* 2014; Zhang *et al.* 2018, 2019), accompanied by fast, strong and random variations of wave frequency and phase (Zhang *et al.* 2020*a*,*b*), often resulting in the formation of almost independent short wave packets or subpackets (Mourenas *et al.* 2018; Zhang *et al.* 2020*a*). Such a chaotization of wave fields is likely partly driven by currents of resonant electrons (Nunn *et al.* 2009; Demekhov 2011; Katoh & Omura 2011, 2016; Tao, Zonca & Chen 2017; Tao *et al.* 2020) and sideband instability (Nunn 1986), as well as by the simultaneous excitation of at least two different waves with a significant frequency difference (Katoh & Omura 2013; Crabtree *et al.* 2017; Zhang *et al.* 2020*b*). Since phase bunching is a local process, wave modulation cannot affect the theoretical model of energy and pitch-angle jumps due to bunching, but the inclusion of such a modulation into the two-wave model map would require some probabilistic distribution of wave amplitudes within short wave packets. The situation is more complicated for phase trapping, which is non-local and depends on wave packet size and amplitude modulation within the packets (Mourenas *et al.* 2018). Test particle simulations demonstrate that wave modulation alone makes phase trapping less efficient for electron acceleration, but increases the probability of phase trapping (Kubota & Omura 2018; Gan *et al.* 2020*a*;

https://doi.org/10.1017/S0022377821000246 Published online by Cambridge University Press

Zhang *et al.* 2020*a*). Thus, an important further development of the mapping technique for nonlinear wave–particle interaction would require modifications of the phase trapping model.

Another important constraint for trapping efficiency is related to the resonance overlapping in the multiwave system. We restrict our consideration to the case of well separated resonances; however, spacecraft observations often report the presence of quite broad-band whistler-mode emission where resonances of two neighbouring waves can overlap (see discussion in, e.g. Summers *et al.* (2014) and Tong *et al.* (2019)). Such resonance overlapping should enhance the electron diffusion, but destroy the phase trapping (e.g. Karimabadi *et al.* 1990; Artemyev *et al.* 2010; Shklyar & Zimbardo 2014). In the absence of trapping resonant systems can be described by the simple Fokker–Plank equation (Lichtenberg & Lieberman 1983; Sagdeev *et al.* 1988), i.e. the mapping technique described within this study can be reduced to a standard map. The most natural partial overlapping would result in a quite complex situation where the assumption of the resonant phase randomization (the basic assumption of the described map) could be violated. Such systems would be described by fractional Fokker–Plank equations (e.g. Zelenyi & Milovanov 2004; Zaslavsky 2005; Isliker, Vlahos & Constantinescu 2017), and this is a poorly investigated topic in application to the physics of resonant wave–particle interaction.

To conclude, we have demonstrated the usefulness of the mapping technique for Hamiltonian systems describing nonlinear resonant interaction of charged particles and intense electromagnetic waves. We have shown that in systems with two (and more) waves, the resonant interaction destroys the symmetries of the single wave resonance and drives a rapid smoothing of particle phase space density gradients. The proposed approach appears very promising for the investigation of relativistic electron interaction with various intense whistler-mode waves and EMIC waves in the Earth's radiation belts (Katoh & Omura 2013; Mourenas *et al.* 2016*a*,*b*; Ma *et al.* 2017; He *et al.* 2020; Yu *et al.* 2020; Zhang *et al.* 2020*b*) or in the solar wind (Wilson *et al.* 2007, 2013; Krafft, Volokitin & Krasnoselskikh 2013; Krafft & Volokitin 2016; Roberg-Clark *et al.* 2019; Tong *et al.* 2019). It could be useful also for studying electron acceleration by simultaneous laser-driven plasma waves (Modena *et al.* 1995; Tikhonchuk 2019), and electron precipitation driven by VLF waves generated by electron beams or antennas in space (Carlsten *et al.* 2019; Borovsky *et al.* 2020).

Editor Hong Qin thanks the referees for their advice in evaluating this article.

Funding

The work of A.V.A., A.I.N. and A.A.V. was supported by Russian Scientific Foundation (project no. 19-12-00313). The work of A.V.A and X.J.Z. was also supported in part by NSF grant 2021749 and NASA grant 80NSSC20K1270. The work of X.J.Z. and D.L.V. was supported by NASA grants 80NSSC20K1578 and 80NSSC19K0266. The work of A.I.N. was supported in part by the Leverhulme Trust grant RPG-2018-143.

Declaration of interests

The authors report no conflict of interest.

Appendix A

Equation (3.6) describes energy decrease due to phase bunching, and natural limitation of this equation is that $\gamma + \Delta\gamma$ should be larger than one; or, alternatively, $I_x +$

https://doi.org/10.1017/S0022377821000246 Published online by Cambridge University Press

$(m_e c^2/\omega)\Delta\gamma$ should be larger than zero. This effect of drift asymmetry, i.e. the absence of electron drift to negative I_x, has been noticed by Lundin & Shkliar (1977) who showed that for very small I_x the phase bunching changes the drift direction. This effect is called anomalous phase bunching (Kitahara & Katoh 2019; Gan *et al.* 2020*a*; Grach & Demekhov 2020) and basically consists in positive I_x (and γ) changes due to bunching at very small I_x. Theoretically, the parametrical boundary of anomalous bunching in energy/pitch-angle space is determined by $I_x < I_x^*$ with I_x^* scaling as $(B_w/B_0)^{2/3}$. Let us derive this scaling, but leave the more detailed consideration of small I_x phase bunching to further consideration. We start with (2.5) written for a single wave

$$H_I = -\omega I + m_e c^2\gamma + \sqrt{\frac{2I\Omega_{ce}}{m_e c^2}}\frac{e}{\gamma}\frac{B_w}{k}\sin\varphi, \quad \gamma = \sqrt{1+\frac{(P+kI)^2}{m_e^2c^2}+\frac{2I\Omega_{ce}}{m_e c^2}}. \quad \text{(A 1}a,b\text{)}$$

Hamiltonian equations for I and φ take the form

$$\dot{I} = -\sqrt{\frac{2I\Omega_{ce}}{m_e c^2}}\frac{eB_w}{k\gamma}\sin\varphi, \quad \dot{\varphi} = \frac{k^2}{\gamma m_e}(I-I_R) + \sqrt{\frac{\Omega_{ce}}{2Im_e c^2}}\frac{eB_w}{k\gamma}\sin\varphi, \qquad \text{(A 2}a,b\text{)}$$

where $I_R = (\gamma\omega m_e - P)/k$ is the solution of $\partial H/\partial I = 0$ equation for $B_w = 0$. Equation (A 2*a*,*b*) describes fast phase rotation (with frequency $k^2(I-I_R)/\gamma m_e$) and I, φ evolution driven by much weaker wave force $\sim B_w/B_0$. Until I (and I_R) is sufficiently large to keep this time separation, we can apply the theory of phase bunching resulting in (3.6). However, let us consider small I, I_R values. We introduce a small parameter $\varepsilon = B_w/B_0$ and normalized $(\tilde{I},\tilde{I}_R) = (I, I_R)/\varepsilon^\beta$

$$\frac{d\tilde{I}}{dt} = -\sqrt{\frac{2\tilde{I}\Omega_{ce}}{m_e c^2}}\frac{eB_0}{k\gamma}\varepsilon^{1-\beta/2}\sin\varphi, \quad \frac{d\varphi}{dt} = \frac{k^2\varepsilon^\beta}{\gamma m_e}(\tilde{I}-\tilde{I}_R) + \sqrt{\frac{\Omega_{ce}}{2\tilde{I}m_e c^2}}\frac{eB_0}{k\gamma}\varepsilon^{1-\beta/2}\sin\varphi. \qquad \text{(A 3}a,b\text{)}$$

Introducing slow time $\tau = t\varepsilon^{1-\beta/2}$, we obtain

$$\frac{d\tilde{I}}{d\tau} = -\sqrt{\frac{2\tilde{I}\Omega_{ce}}{m_e c^2}}\frac{eB_0}{k\gamma}\sin\varphi, \quad \frac{d\varphi}{d\tau} = \frac{k^2}{\gamma m_e}(\tilde{I}-\tilde{I}_R)\varepsilon^{3\beta/2-1} + \sqrt{\frac{\Omega_{ce}}{2\tilde{I}m_e c^2}}\frac{eB_0}{k\gamma}\sin\varphi. \qquad \text{(A 4}a,b\text{)}$$

Thus, for $\beta = 2/3$ (A 4*a*,*b*) lose the small parameter, and $\tilde{I}$, φ would change with the same rate. Then the applicability of equations of the phase bunching theory breaks, and a new model for ΔI (or $\Delta\gamma$, ΔI_x) is required. Here $\beta = 2/3$ gives the threshold value for $I_x \sim I \sim (B_w/B_0)^\beta$.

Appendix B

Figure 8 shows that there are certain domains in the energy/pitch-angle space where electrons resonate with whistler wave nonlinearly. Thus, simulation of resonant electron dynamics should be within these domains. Figure 14(*b*) shows the largest domain that cover all energies and pitch-angles where electrons experience phase bunching. The phase bunching results in energy/pitch-angle change and electron drifts within the domain. An important property of the domain boundary is that $\Delta_{scat}\gamma$ tends there to zero as $\sim (I - I_{boundary})^{4/3}$ where I and $I_{boundary}$ are values of moment and its boundary value (Artemyev *et al.* 2019*a*), i.e. $\Delta\gamma$ drops to zero at the domain boundary and no particles should leave this domain (in absence of diffusion that is characterized by a finite diffusion coefficient

https://doi.org/10.1017/S0022377821000246 Published online by Cambridge University Press

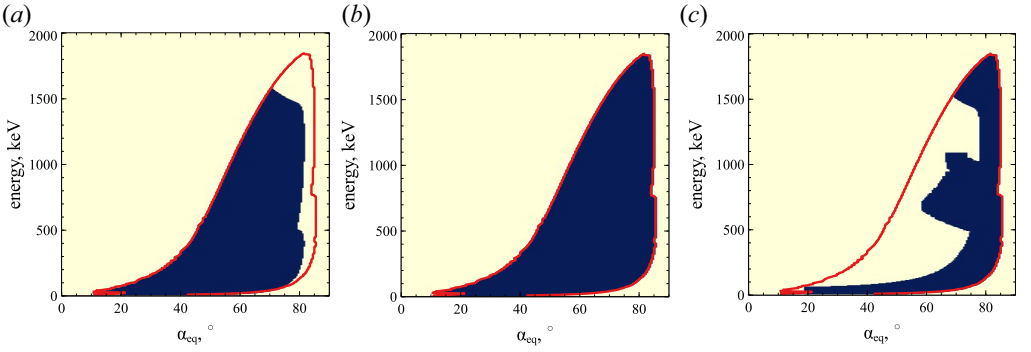


FIGURE 14. Domains in energy/pitch-angle space with: positive probability of trapping (*a*), a finite phase bunching energy/pitch-angle change (*b*), positions of release from the trapping (*c*). Red curve shows boundary of panel (*b*) domain.

within the entire energy/pitch-angle space). As $\Delta_{\rm scat}\gamma$ has been derived numerically, there are possible fluctuations making $\Delta_{\rm scat}\gamma$ finite at the boundary. Thus, distribution $\Delta\gamma(E, \alpha_{\rm eq})$ should be corrected to set $\Delta_{\rm scat}\gamma = 0$ at the domain boundary. Moreover, if during the simulation resonant electrons escape from the domain of phase bunching (e.g. because of numerical effects), these electrons should be returned into the domain (e.g. reflecting them back from the boundary on the same $\Delta_{\rm scat}\gamma$). Note that this procedure is required only in the absence of particle diffusion.[1]

The domain of a finite trapping probability is smaller than the bunching domain (see figure 14*a*). Again, the probability of trapping tends to zero at the phase bunching domain boundary as $\Pi \sim (I - I_{boundary})^{1/3}$ (Artemyev *et al.* 2019*a*), and Π should be set equal to zero on this boundary even if numerical fluctuations of Π evaluation give some finite value. Of course, there are no regions with $\Pi > 0$ outside the phase bunching domain.

Release of trapped electrons from the resonance also should be within the phase bunching domain (see figure 14*c*). Numerical errors put some release locations outside this domain; the trapping variation $\Delta_{\rm trap}\gamma$ should be corrected to move the release locations within the domain. This guarantees that for each energy/pitch-angle within the phase bunching domain we would have incoming and outgoing phase space flows.

REFERENCES

AGAPITOV, O. V., ARTEMYEV, A., KRASNOSELSKIKH, V., KHOTYAINTSEV, Y. V., MOURENAS, D., BREUILLARD, H., BALIKHIN, M. & ROLLAND, G. 2013 Statistics of whistler mode waves in the outer radiation belt: cluster STAFF-SA measurements. *J. Geophys. Res.* **118**, 3407–3420.

AGAPITOV, O. V., ARTEMYEV, A., MOURENAS, D., KRASNOSELSKIKH, V., BONNELL, J., LE CONTEL, O., CULLY, C. M. & ANGELOPOULOS, V. 2014 The quasi-electrostatic mode of chorus waves and electron nonlinear acceleration. *J. Geophys. Res.* **119**, 1606–1626.

AGAPITOV, O. V., ARTEMYEV, A. V., MOURENAS, D., MOZER, F. S. & KRASNOSELSKIKH, V. 2015*a* Empirical model of lower band chorus wave distribution in the outer radiation belt. *J. Geophys. Res.* **120**, 10.

AGAPITOV, O. V., ARTEMYEV, A. V., MOURENAS, D., MOZER, F. S. & KRASNOSELSKIKH, V. 2015*b* Nonlinear local parallel acceleration of electrons through Landau trapping by oblique whistler mode waves in the outer radiation belt. *Geophys. Res. Lett.* **42**, 10.

[1]The system has 3 degrees of freedom. Thus, generally there are deviations from adiabatic trajectories even for non-resonant motions due to the Arnold diffusion (Arnold *et al.* 2006). However, this diffusion is exponentially slow and can be neglected here.

https://doi.org/10.1017/S0022377821000246 Published online by Cambridge University Press

ALBERT, J. M. 1993 Cyclotron resonance in an inhomogeneous magnetic field. *Phys. Fluids* B **5**, 2744–2750.

ALBERT, J. M. 2001 Comparison of pitch angle diffusion by turbulent and monochromatic whistler waves. *J. Geophys. Res*. **106**, 8477–8482.

ALBERT, J. M. 2010 Diffusion by one wave and by many waves. *J. Geophys. Res*. **115**.

ALBERT, J. M., STARKS, M. J., HORNE, R. B., MEREDITH, N. P. & GLAUERT, S. A. 2016 Quasi-linear simulations of inner radiation belt electron pitch angle and energy distributions. *Geophys. Res. Lett*. **43**, 2381–2388.

ALBERT, J. M., TAO, X. & BORTNIK, J. 2013 Aspects of nonlinear wave-particle interactions. In *Dynamics of the Earth's Radiation Belts and Inner Magnetosphere* (ed. D. Summers, I. U. Mann, D. N. Baker & M. Schulz). American Geophysical Union.

ALLANSON, O., WATT, C. E. J., RATCLIFFE, H., ALLISON, H. J., MEREDITH, N. P., BENTLEY, S. N., ROSS, J. P. J. & GLAUERT, S. A. 2020 Particle-in-cell experiments examine electron diffusion by whistler-mode waves: 2. Quasi-linear and nonlinear dynamics. *J. Geophys. Res. (Space Phys.)* **125** (7), e27949.

ANDRONOV, A. A. & TRAKHTENGERTS, V. Y. 1964 Kinetic instability of the earth's outer radiation belt. *Geomagn. Aeron*. **4**, 233–242.

ARNOLD, V. I., KOZLOV, V. V. & NEISHTADT, A. I. 2006 *Mathematical Aspects of Classical and Celestial Mechanics*, 3rd edn. Springer-Verlag.

ARTEMYEV, A. V., AGAPITOV, O., MOURENAS, D., KRASNOSELSKIKH, V., SHASTUN, V. & MOZER, F. 2016*a* Oblique whistler-mode waves in the earth's inner magnetosphere: energy distribution, origins, and role in radiation belt dynamics. *Space Sci. Rev*. **200** (1–4), 261–355.

ARTEMYEV, A. V., NEISHTADT, A. I., VAINCHTEIN, D. L., VASILIEV, A. A., VASKO, I. Y. & ZELENYI, L. M. 2018*a* Trapping (capture) into resonance and scattering on resonance: summary of results for space plasma systems. *Commun. Nonlinear Sci. Numer. Simul*. **65**, 111–160.

ARTEMYEV, A. V., NEISHTADT, A. I. & VASILIEV, A. A. 2019*a* Kinetic equation for nonlinear wave-particle interaction: solution properties and asymptotic dynamics. *Phys.* D *Nonlinear Phenom*. **393**, 1–8. arXiv:1809.03743

ARTEMYEV, A. V., NEISHTADT, A. I. & VASILIEV, A. A. 2020*a* A map for systems with resonant trappings and scatterings. *Regular Chaotic Dyn*. **25** (1), 2–10.

ARTEMYEV, A. V., NEISHTADT, A. I. & VASILIEV, A. A. 2020*b* Mapping for nonlinear electron interaction with whistler-mode waves. *Phys. Plasmas* **27** (4), 042902. arXiv:1911.11459

ARTEMYEV, A. V., NEISHTADT, A. I., VASILIEV, A. A. & MOURENAS, D. 2016*b* Kinetic equation for nonlinear resonant wave-particle interaction. *Phys. Plasmas* **23** (9), 090701.

ARTEMYEV, A. V., NEISHTADT, A. I., VASILIEV, A. A. & MOURENAS, D. 2017 Probabilistic approach to nonlinear wave-particle resonant interaction. *Phys. Rev.* E **95** (2), 023204.

ARTEMYEV, A. V., NEISHTADT, A. I., VASILIEV, A. A. & MOURENAS, D. 2018*b* Long-term evolution of electron distribution function due to nonlinear resonant interaction with whistler mode waves. *J. Plasma Phys*. **84**, 905840206.

ARTEMYEV, A. V., NEISHTADT, A. I., ZELENYI, L. M. & VAINCHTEIN, D. L. 2010 Adiabatic description of capture into resonance and surfatron acceleration of charged particles by electromagnetic waves. *Chaos* **20** (4), 043128.

ARTEMYEV, A. V., VASILIEV, A. A., MOURENAS, D., AGAPITOV, O. & KRASNOSELSKIKH, V. 2013 Nonlinear electron acceleration by oblique whistler waves: Landau resonance vs. cyclotron resonance. *Phys. Plasmas* **20**, 122901.

ARTEMYEV, A. V., VASILIEV, A. A., MOURENAS, D., AGAPITOV, O. V. & KRASNOSELSKIKH, V. V. 2014*a* Electron scattering and nonlinear trapping by oblique whistler waves: the critical wave intensity for nonlinear effects. *Phys. Plasmas* **21** (10), 102903.

ARTEMYEV, A. V., VASILIEV, A. A., MOURENAS, D., AGAPITOV, O., KRASNOSELSKIKH, V., BOSCHER, D. & ROLLAND, G. 2014*b* Fast transport of resonant electrons in phase space due to nonlinear trapping by whistler waves. *Geophys. Res. Lett*. **41**, 5727–5733.

ARTEMYEV, A. V., VASILIEV, A. A., MOURENAS, D., NEISHTADT, A. I., AGAPITOV, O. V. & KRASNOSELSKIKH, V. 2015 Probability of relativistic electron trapping by parallel and oblique whistler-mode waves in earth's radiation belts. *Phys. Plasmas* **22** (11), 112903.

https://doi.org/10.1017/S0022377821000246 Published online by Cambridge University Press

ARTEMYEV, A. V., VASILIEV, A. A. & NEISHTADT, A. I. 2019*b* Charged particle nonlinear resonance with localized electrostatic wave-packets. *Commun. Nonlinear Sci. Numer. Simul*. **72**, 392–406.

BALIKHIN, M. A., DE WIT, T. D., ALLEYNE, H. S. C. K., WOOLLISCROFT, L. J. C., WALKER, S. N., KRASNOSEL'SKIKH, V., MIER-JEDRZEJEOWICZ, W. A. C. & BAUMJOHANN, W. 1997 Experimental determination of the dispersion of waves observed upstream of a quasi-perpendicular shock. *Geophys. Res. Lett*. **24**, 787–790.

BELL, T. F. 1984 The nonlinear gyroresonance interaction between energetic electrons and coherent VLF waves propagating at an arbitrary angle with respect to the earth's magnetic field. *J. Geophys. Res*. **89**, 905–918.

BENKADDA, S., SEN, A. & SHKLYAR, D. R. 1996 Chaotic dynamics of charged particles in the field of two monochromatic waves in a magnetized plasma. *Chaos* **6** (3), 451–460.

BOROVSKY, J. E., DELZANNO, G. L., DORS, E. E., THOMSEN, M. F., SANCHEZ, E. R., HENDERSON, M. G., MARSHALL, R. A., GILCHRIST, B. E., MIARS, G., CARLSTEN, B. E., *et al.* 2020 Solving the auroral-arc-generator question by using an electron beam to unambiguously connect critical magnetospheric measurements to auroral images. *J. Atmos. Sol.-Terr. Phys*. **206**, 105310.

CAMPOREALE, E. & ZIMBARDO, G. 2015 Wave-particle interactions with parallel whistler waves: nonlinear and time-dependent effects revealed by particle-in-cell simulations. *Phys. Plasmas* **22** (9), 092104. arXiv:1412.3229

CARLSTEN, B. E., COLESTOCK, P. L., CUNNINGHAM, G. S., DELZANNO, G. L., DORS, E. E., HOLLOWAY, M. A., JEFFERY, C. A., LEWELLEN, J. W., MARKSTEINER, Q. R., NGUYEN, D. C., *et al.* 2019 Radiation-belt remediation using space-based antennas and electron beams. *IEEE Trans. Plasma Sci*. **47** (5), 2045–2063.

CATTELL, C. A., BRENEMAN, A. W., THALLER, S. A., WYGANT, J. R., KLETZING, C. A. & KURTH, W. S. 2015 Van Allen probes observations of unusually low frequency whistler mode waves observed in association with moderate magnetic storms: statistical study. *Geophys. Res. Lett*. **42**, 7273–7281.

CATTELL, C., WYGANT, J. R., GOETZ, K., KERSTEN, K., KELLOGG, P. J., VON ROSENVINGE, T., BALE, S. D., ROTH, I., TEMERIN, M., HUDSON, M. K., *et al.* 2008 Discovery of very large amplitude whistler-mode waves in earth's radiation belts. *Geophys. Res. Lett*. **35**, 1105.

CHASTON, C. C., SALEM, C., BONNELL, J. W., CARLSON, C. W., ERGUN, R. E., STRANGEWAY, R. J. & MCFADDEN, J. P. 2008 The turbulent Alfvénic aurora. *Phys. Rev. Lett*. **100** (17), 175003.

CHEN, L., BRENEMAN, A. W., XIA, Z. & ZHANG, X.-J. 2020 Modeling of bouncing electron microbursts induced by ducted chorus waves. *Geophys. Res. Lett*. **47** (17), e89400.

CHEN, L., ZHU, H. & ZHANG, X. 2019 Wavenumber analysis of EMIC waves. *Geophys. Res. Lett*. **46** (11), 5689–5697.

CHIRIKOV, B. V. 1979 A universal instability of many-dimensional oscillator systems. *Phys. Rep*. **52**, 263–379.

CRABTREE, C., TEJERO, E., GANGULI, G., HOSPODARSKY, G. B. & KLETZING, C. A. 2017 Bayesian spectral analysis of chorus subelements from the Van Allen Probes. *J. Geophys. Res. (Space Phys.)* **122** (6), 6088–6106.

CULLY, C. M., ANGELOPOULOS, V., AUSTER, U., BONNELL, J. & LE CONTEL, O. 2011 Observational evidence of the generation mechanism for rising-tone chorus. *Geophys. Res. Lett*. **38**, 1106.

CULLY, C. M., BONNELL, J. W. & ERGUN, R. E. 2008 THEMIS observations of long-lived regions of large-amplitude whistler waves in the inner magnetosphere. *Geophys. Res. Lett*. **35**, 17.

DEMEKHOV, A. G. 2011 Generation of VLF emissions with the increasing and decreasing frequency in the magnetosperic cyclotron maser in the backward wave oscillator regime. *Radiophys. Quant. Electron*. **53**, 609–622.

DEMEKHOV, A. G., TRAKHTENGERTS, V. Y., RYCROFT, M. J. & NUNN, D. 2006 Electron acceleration in the magnetosphere by whistler-mode waves of varying frequency. *Geomagn. Aeron*. **46**, 711–716.

DEMEKHOV, A. G., TRAKHTENGERTS, V. Y., RYCROFT, M. & NUNN, D. 2009 Efficiency of electron acceleration in the earth's magnetosphere by whistler mode waves. *Geomagn. Aeron*. **49**, 24–29.

https://doi.org/10.1017/S0022377821000246 Published online by Cambridge University Press

Drozdov, A. Y., Shprits, Y. Y., Orlova, K. G., Kellerman, A. C., Subbotin, D. A., Baker, D. N., Spence, H. E. & Reeves, G. D. 2015 Energetic, relativistic, and ultrarelativistic electrons: comparison of long-term VERB code simulations with Van Allen Probes measurements. *J. Geophys. Res*. **120**, 3574–3587.

Drummond, W. E. & Pines, D. 1962 Nonlinear stability of plasma oscillations. *Nucl. Fusion Suppl*. **3**, 1049–1058.

Foster, J. C., Erickson, P. J., Baker, D. N., Claudepierre, S. G., Kletzing, C. A., Kurth, W., Reeves, G. D., Thaller, S. A., Spence, H. E., Shprits, Y. Y., *et al.* 2014 Prompt energization of relativistic and highly relativistic electrons during a substorm interval: Van Allen Probes observations. *Geophys. Res. Lett*. **41**, 20–25.

Furuya, N., Omura, Y. & Summers, D. 2008 Relativistic turning acceleration of radiation belt electrons by whistler mode chorus. *J. Geophys. Res*. **113**, 4224.

Gan, L., Li, W., Ma, Q., Albert, J. M., Artemyev, A. V. & Bortnik, J. 2020*a* Nonlinear interactions between radiation belt electrons and chorus waves: dependence on wave amplitude modulation. *Geophys. Res. Lett*. **47** (4), e85987.

Gan, L., Li, W., Ma, Q., Artemyev, A. V. & Albert, J. M. 2020*b* Unraveling the formation mechanism for the bursts of electron butterfly distributions: test particle and quasilinear simulations. *Geophys. Res. Lett*. **47** (21), e90749.

Gelfreich, V., Rom-Kedar, V., Shah, K. & Turaev, D. 2011 Robust exponential acceleration in time-dependent billiards. *Phys. Rev. Lett*. **106** (7), 074101.

Grach, V. S. & Demekhov, A. G. 2018 Resonance interaction of relativistic electrons with ion-cyclotron waves. I. Specific features of the nonlinear interaction regimes. *Radiophys. Quant. Electron*. **60** (12), 942–959.

Grach, V. S. & Demekhov, A. G. 2020 Precipitation of relativistic electrons under resonant interaction with electromagnetic ion cyclotron wave packets. *J. Geophys. Res. (Space Phys.)* **125** (2), e27358.

He, Z., Yan, Q., Zhang, X., Yu, J., Ma, Y., Cao, Y. & Cui, J. 2020 Precipitation loss of radiation belt electrons by two-band plasmaspheric hiss waves. *J. Geophys. Res. (Space Phys.)* **125**, e2020JA028157.

Hiraga, R. & Omura, Y. 2020 Acceleration mechanism of radiation belt electrons through interaction with multi-subpacket chorus waves. *Earth Planet. Space* **72** (1), 21.

Hsieh, Y.-K., Kubota, Y. & Omura, Y. 2020 Nonlinear evolution of radiation belt electron fluxes interacting with oblique whistler mode chorus emissions. *J. Geophys. Res.: Space Phys*. e2019JA027465.

Hsieh, Y.-K. & Omura, Y. 2017*a* Nonlinear dynamics of electrons interacting with oblique whistler mode chorus in the magnetosphere. *J. Geophys. Res*. **122**, 675–694.

Hsieh, Y.-K. & Omura, Y. 2017*b* Study of wave-particle interactions for whistler mode waves at oblique angles by utilizing the gyroaveraging method. *Radio Sci*. **52** (10), 1268–1281.

Isliker, H., Vlahos, L. & Constantinescu, D. 2017 Fractional transport in strongly turbulent plasmas. *Phys. Rev. Lett*. **119** (4), 045101. arXiv:1707.01526

Itin, A. P. & Neishtadt, A. I. 2012 Fermi acceleration in time-dependent rectangular billiards due to multiple passages through resonances. *Chaos* **22** (2), 026119. arXiv:1112.3472

Itin, A. P., Neishtadt, A. I. & Vasiliev, A. A. 2000 Captures into resonance and scattering on resonance in dynamics of a charged relativistic particle in magnetic field and electrostatic wave. *Phys.* D*: Nonlinear Phenom*. **141**, 281–296.

Karimabadi, H., Akimoto, K., Omidi, N. & Menyuk, C. R. 1990 Particle acceleration by a wave in a strong magnetic field - regular and stochastic motion. *Phys. Fluids* B **2**, 606–628.

Karpman, V. I. 1974 Nonlinear effects in the ELF waves propagating along the magnetic field in the magnetosphere. *Space Sci. Rev*. **16**, 361–388.

Katoh, Y. 2014 A simulation study of the propagation of whistler-mode chorus in the Earth's inner magnetosphere. *Earth Planet. Space* **66**, 6.

Katoh, Y. & Omura, Y. 2011 Amplitude dependence of frequency sweep rates of whistler mode chorus emissions. *J. Geophys. Res*. **116**, 7201.

https://doi.org/10.1017/S0022377821000246 Published online by Cambridge University Press

KATOH, Y. & OMURA, Y. 2013 Effect of the background magnetic field inhomogeneity on generation processes of whistler-mode chorus and broadband hiss-like emissions. *J. Geophys. Res*. **118**, 4189–4198.

KATOH, Y. & OMURA, Y. 2016 Electron hybrid code simulation of whistler-mode chorus generation with real parameters in the Earth's inner magnetosphere. *Earth Planet. Space* **68** (1), 192.

KENNEL, C. F. & ENGELMANN, F. 1966 Velocity space diffusion from weak plasma turbulence in a magnetic field. *Phys. Fluids* **9**, 2377–2388.

KERSTEN, T., HORNE, R. B., GLAUERT, S. A., MEREDITH, N. P., FRASER, B. J. & GREW, R. S. 2014 Electron losses from the radiation belts caused by EMIC waves. *J. Geophys. Res*. **119**, 8820–8837.

KHAZANOV, G. V., TEL'NIKHIN, A. A. & KRONBERG, T. K. 2013 Radiation belt electron dynamics driven by large-amplitude whistlers. *J. Geophys. Res. (Space Phys.)* **118** (10), 6397–6404.

KHAZANOV, G. V., TEL'NIKHIN, A. A. & KRONBERG, T. K. 2014 Stochastic electron motion driven by space plasma waves. *Nonlinear Process. Geophys*. **21** (1), 61–85.

KITAHARA, M. & KATOH, Y. 2019 Anomalous trapping of low pitch angle electrons by coherent whistler mode waves. *J. Geophys. Res*. **124** (7), 5568–5583.

KLETZING, C. A., KURTH, W. S., ACUNA, M., MACDOWALL, R. J., TORBERT, R. B., AVERKAMP, T., BODET, D., BOUNDS, S. R., CHUTTER, M., CONNERNEY, J., *et al.* 2013 The electric and magnetic field instrument suite and integrated science (EMFISIS) on RBSP. *Space Sci. Rev*. **179**, 127–181.

KRAFFT, C. & VOLOKITIN, A. S. 2016 Electron acceleration by langmuir waves produced by a decay cascade. *Astrophys. J*. **821**, 99.

KRAFFT, C., VOLOKITIN, A. S. & KRASNOSELSKIKH, V. V. 2013 Interaction of energetic particles with waves in strongly inhomogeneous solar wind plasmas. *Astrophys. J*. **778**, 111.

KUBOTA, Y. & OMURA, Y. 2017 Rapid precipitation of radiation belt electrons induced by EMIC rising tone emissions localized in longitude inside and outside the plasmapause. *J. Geophys. Res. (Space Phys.)* **122** (1), 293–309.

KUBOTA, Y. & OMURA, Y. 2018 Nonlinear dynamics of radiation belt electrons interacting with chorus emissions localized in longitude. *J. Geophys. Res. (Space Phys.)* **123**, 4835–4857.

KUBOTA, Y., OMURA, Y. & SUMMERS, D. 2015 Relativistic electron precipitation induced by EMIC-triggered emissions in a dipole magnetosphere. *J. Geophys. Res. (Space Phys.)* **120** (6), 4384–4399.

KUZICHEV, I. V., VASKO, I. Y., RUALDO SOTO-CHAVEZ, A., TONG, Y., ARTEMYEV, A. V., BALE, S. D. & SPITKOVSKY, A. 2019 Nonlinear evolution of the whistler heat flux instability. *Astrophys. J*. **882** (2), 81. arXiv:1907.04878

LE QUEAU, D. & ROUX, A. 1987 Quasi-monochromatic wave-particle interactions in magnetospheric plasmas. *Solar Phys*. **111**, 59–80.

LEONCINI, X., VASILIEV, A. & ARTEMYEV, A. 2018 Resonance controlled transport in phase space. *Phys.* D *Nonlinear Phenom*. **364**, 22–26.

LERCHE, I. 1968 Quasilinear theory of resonant diffusion in a magneto-active, relativistic plasma. *Phys. Fluids* **11**.

LI, W., SANTOLIK, O., BORTNIK, J., THORNE, R. M., KLETZING, C. A., KURTH, W. S. & HOSPODARSKY, G. B. 2016 New chorus wave properties near the equator from Van Allen Probes wave observations. *Geophys. Res. Lett*. **43**, 4725–4735.

LI, W., THORNE, R. M., MA, Q., NI, B., BORTNIK, J., BAKER, D. N., SPENCE, H. E., REEVES, G. D., KANEKAL, S. G., GREEN, J. C., *et al.* 2014 Radiation belt electron acceleration by chorus waves during the 17 March 2013 storm. *J. Geophys. Res*. **119**, 4681–4693.

LICHTENBERG, A. J. & LIEBERMAN, M. A. 1983 *Regular and Stochastic Motion*, Applied Mathematical Sciences. Springer.

LUNDIN, B. V. & SHKLIAR, D. R. 1977 Interaction of electrons with low transverse velocities with VLF waves in an inhomogeneous plasma. *Geomagn. Aeron*. **17**, 246–251.

LYONS, L. R. & WILLIAMS, D. J. 1984 *Quantitative Aspects of Magnetospheric Physics*. Reidel Publishing Company.

MA, Q., LI, W., BORTNIK, J., THORNE, R. M., CHU, X., OZEKE, L. G., REEVES, G. D., KLETZING, C. A., KURTH, W. S., HOSPODARSKY, G. B., *et al.* 2018 Quantitative evaluation

https://doi.org/10.1017/S0022377821000246 Published online by Cambridge University Press

of radial diffusion and local acceleration processes during GEM challenge events. *J. Geophys. Res. (Space Phys.)* **123** (3), 1938–1952.

MA, Q., LI, W., THORNE, R. M., NISHIMURA, Y., ZHANG, X.-J., REEVES, G. D., KLETZING, C. A., KURTH, W. S., HOSPODARSKY, G. B., HENDERSON, M. G., *et al.* 2016 Simulation of energy-dependent electron diffusion processes in the Earth's outer radiation belt. *J. Geophys. Res*. **121**, 4217–4231.

MA, Q., MOURENAS, D., LI, W., ARTEMYEV, A. & THORNE, R. M. 2017 VLF waves from ground-based transmitters observed by the Van Allen Probes: statistical model and effects on plasmaspheric electrons. *Geophys. Res. Lett*. **44**, 6483–6491.

MAUK, B. H., FOX, N. J., KANEKAL, S. G., KESSEL, R. L., SIBECK, D. G. & UKHORSKIY, A. 2013 Science objectives and rationale for the radiation belt storm probes mission. *Space Sci. Rev*. **179**, 3–27.

MAUK, B. H., HAGGERTY, D. K., PARANICAS, C., CLARK, G., KOLLMANN, P., RYMER, A. M., BOLTON, S. J., LEVIN, S. M., ADRIANI, A., ALLEGRINI, F., *et al.* 2017 Discrete and broadband electron acceleration in Jupiter's powerful aurora. *Nature* **549** (7670), 66–69.

MEANS, J. D. 1972 Use of the three-dimensional covariance matrix in analyzing the polarization properties of plane waves. *J. Geophys. Res*. **77**, 5551.

MENIETTI, J. D., SHPRITS, Y. Y., HORNE, R. B., WOODFIELD, E. E., HOSPODARSKY, G. B. & GURNETT, D. A. 2012 Chorus, ECH, and Z mode emissions observed at Jupiter and Saturn and possible electron acceleration. *J. Geophys. Res*. **117**, A12214.

MEREDITH, N. P., HORNE, R. B., GLAUERT, S. A. & ANDERSON, R. R. 2007 Slot region electron loss timescales due to plasmaspheric hiss and lightning-generated whistlers. *J. Geophys. Res*. **112**, 8214.

MILLAN, R. M. & THORNE, R. M. 2007 Review of radiation belt relativistic electron losses. *J. Atmos. Sol.-Terr. Phys*. **69**, 362–377.

MODENA, A., NAJMUDIN, Z., DANGOR, A. E., CLAYTON, C. E., MARSH, K. A., JOSHI, C., MALKA, V., DARROW, C. B., DANSON, C., NEELY, D., *et al.* 1995 Electron acceleration from the breaking of relativistic plasma waves. *Nature* **377** (6550), 606–608.

MOURENAS, D., ARTEMYEV, A., AGAPITOV, O. & KRASNOSELSKIKH, V. 2012 Acceleration of radiation belts electrons by oblique chorus waves. *J. Geophys. Res*. **117**, 10212.

MOURENAS, D., ARTEMYEV, A. V., AGAPITOV, O. V., KRASNOSELSKIKH, V. & MOZER, F. S. 2015 Very oblique whistler generation by low-energy electron streams. *J. Geophys. Res*. **120**, 3665–3683.

MOURENAS, D., ARTEMYEV, A. V., AGAPITOV, O. V., MOZER, F. S. & KRASNOSELSKIKH, V. V. 2016*a* Equatorial electron loss by double resonance with oblique and parallel intense chorus waves. *J. Geophys. Res*. **121**, 4498–4517.

MOURENAS, D., ARTEMYEV, A. V., MA, Q., AGAPITOV, O. V. & LI, W. 2016*b* Fast dropouts of multi-MeV electrons due to combined effects of EMIC and whistler mode waves. *Geophys. Res. Lett*. **43** (9), 4155–4163.

MOURENAS, D., ZHANG, X.-J., ARTEMYEV, A. V., ANGELOPOULOS, V., THORNE, R. M., BORTNIK, J., NEISHTADT, A. I. & VASILIEV, A. A. 2018 Electron nonlinear resonant interaction with short and intense parallel chorus wave packets. *J. Geophys. Res*. **123**, 4979–4999.

NEISHTADT, A. I. 1999 On adiabatic invariance in two-frequency systems. In *Hamiltonian Systems with Three or More Degrees of Freedom* (ed. C. Simo), NATO ASI Series C, vol. 533, pp. 193–213. Kluwer Academic Publishers.

NEISHTADT, A. I. 2014 Averaging, passage through resonances, and capture into resonance in two-frequency systems. *Russian Math. Surv*. **69** (5), 771.

NEISHTADT, A. I. & VASILIEV, A. A. 2006 Destruction of adiabatic invariance at resonances in slow fast Hamiltonian systems. *Nucl. Instrum. Meth. Phys. Res.* A **561**, 158–165. arXiv:arXiv:nlin/0511050

NI, B., THORNE, R. M., ZHANG, X., BORTNIK, J., PU, Z., XIE, L., HU, Z.-J., HAN, D., SHI, R., ZHOU, C., *et al.* 2016 Origins of the Earth's diffuse auroral precipitation. *Space Sci. Rev*. **200**, 205–259.

NISHIMURA, Y., BORTNIK, J., LI, W., THORNE, R. M., LYONS, L. R., ANGELOPOULOS, V., MENDE, S. B., BONNELL, J. W., LE CONTEL, O., CULLY, C., *et al.* 2010 Identifying the driver of pulsating aurora. *Science* **330**, 81–84.

NUNN, D. 1986 A nonlinear theory of sideband stability in ducted whistler mode waves. *Planet. Space Sci*. **34**, 429–451.

https://doi.org/10.1017/S0022377821000246 Published online by Cambridge University Press

NUNN, D. & OMURA, Y. 2012 A computational and theoretical analysis of falling frequency VLF emissions. *J. Geophys. Res*. **117**, 8228.

NUNN, D. & OMURA, Y. 2015 A computational and theoretical investigation of nonlinear wave-particle interactions in oblique whistlers. *J. Geophys. Res*. **120**, 2890–2911.

NUNN, D., SANTOLIK, O., RYCROFT, M. & TRAKHTENGERTS, V. 2009 On the numerical modelling of VLF chorus dynamical spectra. *Ann. Geophys*. **27**, 2341–2359.

OMURA, Y., FURUYA, N. & SUMMERS, D. 2007 Relativistic turning acceleration of resonant electrons by coherent whistler mode waves in a dipole magnetic field. *J. Geophys. Res*. **112**, 6236.

OMURA, Y., KATOH, Y. & SUMMERS, D. 2008 Theory and simulation of the generation of whistler-mode chorus. *J. Geophys. Res*. **113**, 4223.

OMURA, Y., MATSUMOTO, H., NUNN, D. & RYCROFT, M. J. 1991 A review of observational, theoretical and numerical studies of VLF triggered emissions. *J. Atmos. Terr. Phys*. **53**, 351–368.

OMURA, Y., MIYASHITA, Y., YOSHIKAWA, M., SUMMERS, D., HIKISHIMA, M., EBIHARA, Y. & KUBOTA, Y. 2015 Formation process of relativistic electron flux through interaction with chorus emissions in the Earth's inner magnetosphere. *J. Geophys. Res*. **120**, 9545–9562.

OMURA, Y., NUNN, D. & SUMMERS, D. 2013 Generation processes of whistler mode chorus emissions: current status of nonlinear wave growth theory. In *Dynamics of the Earth's Radiation Belts and Inner Magnetosphere* (ed. D. Summers, I. U. Mann, D. N. Baker & M. Schulz), pp. 243–254. American Geophysical Union.

PALMADESSO, P. J. 1972 Resonance, particle trapping, and Landau damping in finite amplitude obliquely propagating waves. *Phys. Fluids* **15**, 2006–2013.

ROBERG-CLARK, G. T., AGAPITOV, O., DRAKE, J. F. & SWISDAK, M. 2019 Scattering of energetic electrons by heat-flux-driven whistlers in flares. *Astrophys. J*. **887** (2), 190. arXiv:1908.06481

RYUTOV, D. D. 1969 Quasilinear relaxation of an electron beam in an inhomogeneous plasma. *Sov. J. Expl Theor. Phys*. **30**, 131.

SAGDEEV, R. Z., USIKOV, D. A. & ZASLAVSKY, G. M. 1988 *Nonlinear Physics. From the Pendulum to Turbulence and Chaos*, Contemporary Concepts in Physics. Harwood Academic Publishers.

SANTOLIK, O., KLETZING, C. A., KURTH, W. S., HOSPODARSKY, G. B. & BOUNDS, S. R. 2014 Fine structure of large-amplitude chorus wave packets. *Geophys. Res. Lett*. **41**, 293–299.

SHAPIRO, V. D. & SAGDEEV, R. Z. 1997 Nonlinear wave-particle interaction and conditions for the applicability of quasilinear theory. *Phys. Rep*. **283**, 49–71.

SHEELEY, B. W., MOLDWIN, M. B., RASSOUL, H. K. & ANDERSON, R. R. 2001 An empirical plasmasphere and trough density model: CRRES observations. *J. Geophys. Res*. **106**, 25631–25642.

SHKLYAR, D. R. 1981 Stochastic motion of relativistic particles in the field of a monochromatic wave. *Sov. Phys. JETP* **53**, 1197–1192.

SHKLYAR, D. R. 2011 On the nature of particle energization via resonant wave-particle interaction in the inhomogeneous magnetospheric plasma. *Ann. Geophys*. **29**, 1179–1188.

SHKLYAR, D. R. & MATSUMOTO, H. 2009 Oblique whistler-mode waves in the inhomogeneous magnetospheric plasma: resonant interactions with energetic charged particles. *Surv. Geophys*. **30**, 55–104.

SHKLYAR, D. R. & ZIMBARDO, G. 2014 Particle dynamics in the field of two waves in a magnetoplasma. *Plasma Phys. Control. Fusion* **56** (9), 095002.

SHPRITS, Y. Y., DROZDOV, A. Y., SPASOJEVIC, M., KELLERMAN, A. C., USANOVA, M. E., ENGEBRETSON, M. J., AGAPITOV, O. V., ZHELAVSKAYA, I. S., RAITA, T. J., SPENCE, H. E., *et al.* 2016 Wave-induced loss of ultra-relativistic electrons in the Van Allen radiation belts. *Nat. Commun*. **7**, 12883.

SHPRITS, Y. Y., SUBBOTIN, D. A., MEREDITH, N. P. & ELKINGTON, S. R. 2008 Review of modeling of losses and sources of relativistic electrons in the outer radiation belt II: local acceleration and loss. *J. Atmos. Sol.-Terr. Phys*. **70**, 1694–1713.

SILIN, I., MANN, I. R., SYDORA, R. D., SUMMERS, D. & MACE, R. L. 2011 Warm plasma effects on electromagnetic ion cyclotron wave MeV electron interactions in the magnetosphere. *J. Geophys. Res. (Space Phys.)* **116** (A5), A05215.

https://doi.org/10.1017/S0022377821000246 Published online by Cambridge University Press

Solovev, V. V. & Shkliar, D. R. 1986 Particle heating by a low-amplitude wave in an inhomogeneous magnetoplasma. *Sov. Phys. JETP* **63**, 272–277.

Stix, T. H. 1962 *The Theory of Plasma Waves*. McGraw-Hill.

Summers, D., Omura, Y., Nakamura, S. & Kletzing, C. A. 2014 Fine structure of plasmaspheric hiss. *J. Geophys. Res*. **119**, 9134–9149.

Summers, D. & Thorne, R. M. 2003 Relativistic electron pitch-angle scattering by electromagnetic ion cyclotron waves during geomagnetic storms. *J. Geophys. Res*. **108**, 1143.

Summers, D., Thorne, R. M. & Xiao, F. 1998 Relativistic theory of wave-particle resonant diffusion with application to electron acceleration in the magnetosphere. *J. Geophys. Res*. **103**, 20487–20500.

Tao, X. 2014 A numerical study of chorus generation and the related variation of wave intensity using the DAWN code. *J. Geophys. Res. (Space Phys.)* **119** (5), 3362–3372.

Tao, X. & Bortnik, J. 2010 Nonlinear interactions between relativistic radiation belt electrons and oblique whistler mode waves. *Nonlinear Process. Geophys*. **17**, 599–604.

Tao, X., Bortnik, J., Albert, J. M. & Thorne, R. M. 2012*a* Comparison of bounce-averaged quasi-linear diffusion coefficients for parallel propagating whistler mode waves with test particle simulations. *J. Geophys. Res*. **117**, 10205.

Tao, X., Bortnik, J., Albert, J. M., Thorne, R. M. & Li, W. 2013 The importance of amplitude modulation in nonlinear interactions between electrons and large amplitude whistler waves. *J. Atmos. Sol.-Terr. Phys*. **99**, 67–72.

Tao, X., Li, W., Bortnik, J., Thorne, R. M. & Angelopoulos, V. 2012*b* Comparison between theory and observation of the frequency sweep rates of equatorial rising tone chorus. *Geophys. Res. Lett*. **39** (8), L08106.

Tao, X., Zonca, F. & Chen, L. 2017 Identify the nonlinear wave-particle interaction regime in rising tone chorus generation. *Geophys. Res. Lett*. **44** (8), 3441–3446.

Tao, X., Zonca, F., Chen, L. & Wu, Y. 2020 Theoretical and numerical studies of chorus waves: a review. *Sci. China Earth Sci*. **63** (1), 78–92.

Thorne, R. M. 2010 Radiation belt dynamics: the importance of wave-particle interactions. *Geophys. Res. Lett*. **372**, 22107.

Thorne, R. M. & Kennel, C. F. 1971 Relativistic electron precipitation during magnetic storm main phase. *J. Geophys. Res*. **76**, 4446.

Thorne, R. M., Li, W., Ni, B., Ma, Q., Bortnik, J., Chen, L., Baker, D. N., Spence, H. E., Reeves, G. D., Henderson, M. G., *et al.* 2013 Rapid local acceleration of relativistic radiation-belt electrons by magnetospheric chorus. *Nature* **504**, 411–414.

Thorne, R. M., Ni, B., Tao, X., Horne, R. B. & Meredith, N. P. 2010 Scattering by chorus waves as the dominant cause of diffuse auroral precipitation. *Nature* **467**, 943–946.

Tikhonchuk, V. T. 2019 Physics of laser plasma interaction and particle transport in the context of inertial confinement fusion. *Nucl. Fusion* **59** (3), 032001.

Titova, E. E., Kozelov, B. V., Jiricek, F., Smilauer, J., Demekhov, A. G. & Trakhtengerts, V. Y. 2003 Verification of the backward wave oscillator model of VLF chorus generation using data from MAGION 5 satellite. *Ann. Geophys*. **21**, 1073–1081.

Tong, Y., Vasko, I. Y., Artemyev, A. V., Bale, S. D. & Mozer, F. S. 2019 Statistical study of whistler waves in the solar wind at 1 AU. *Astrophys. J*. **878** (1), 41. arXiv:1905.08958

Tyler, E., Breneman, A., Cattell, C., Wygant, J., Thaller, S. & Malaspina, D. 2019 Statistical occurrence and distribution of high-amplitude whistler mode waves in the outer radiation belt. *Geophys. Res. Lett*. **46** (5), 2328–2336.

Vainchtein, D., Zhang, X.-J., Artemyev, A., Mourenas, D., Angelopoulos, V. & Thorne, R. M. 2018 Evolution of electron distribution driven by nonlinear resonances with intense field-aligned chorus waves. *J. Geophys. Res*. **123**, 8149–8169. doi:10.1029/2018JA025654.

Van Kampen, N. G. 2003 *Stochastic Processes in Physics and Chemistry*, 3rd edn. North Holland.

Vasilev, A. A., Zaslavskii, G. M., Natenzon, M. I., Neishtadt, A. I. & Petrovichev, B. A. 1988 Attractors and stochastic attractors of motion in a magnetic field. *Zh. Eksp. Teor. Fiz*. **94**, 170–187.

Vedenov, A. A., Velikhov, E. & Sagdeev, R. 1962 Quasilinear theory of plasma oscillations. *Nuclear Fusion Suppl*. **2**, 465–475.

https://doi.org/10.1017/S0022377821000246 Published online by Cambridge University Press

WANG, R., VASKO, I. Y., MOZER, F. S., BALE, S. D., ARTEMYEV, A. V., BONNELL, J. W., ERGUN, R., GILES, B., LINDQVIST, P. A., RUSSELL, C. T., *et al.* 2020 Electrostatic turbulence and Debye-scale structures in collisionless shocks. *Astrophys. J. Lett*. **889** (1), L9. arXiv:1912.01770

WATT, C. E. J. & RANKIN, R. 2009 Electron trapping in shear Alfvén waves that power the aurora. *Phys. Rev. Lett*. **102** (4), 045002.

WILSON, L. B. III, CATTELL, C., KELLOGG, P. J., GOETZ, K., KERSTEN, K., HANSON, L., MACGREGOR, R. & KASPER, J. C. 2007 Waves in interplanetary shocks: a wind/WAVES study. *Phys. Rev. Lett*. **99** (4), 041101.

WILSON, L. B. III, CATTELL, C., KELLOGG, P. J., WYGANT, J. R., GOETZ, K., BRENEMAN, A. & KERSTEN, K. 2011 The properties of large amplitude whistler mode waves in the magnetosphere: propagation and relationship with geomagnetic activity. *Geophys. Res. Lett*. **38**, 17107.

WILSON, L. B. III, KOVAL, A., SZABO, A., BRENEMAN, A., CATTELL, C. A., GOETZ, K., KELLOGG, P. J., KERSTEN, K., KASPER, J. C., MARUCA, B. A., *et al.* 2012 Observations of electromagnetic whistler precursors at supercritical interplanetary shocks. *Geophys. Res. Lett*. **39**, 8109.

WILSON, L. B., KOVAL, A., SZABO, A., BRENEMAN, A., CATTELL, C. A., GOETZ, K., KELLOGG, P. J., KERSTEN, K., KASPER, J. C., MARUCA, B. A., *et al.* 2013 Electromagnetic waves and electron anisotropies downstream of supercritical interplanetary shocks. *J. Geophys. Res*. **118**, 5–16. arXiv:1207.6429

YOON, P. H., SEOUGH, J., SALEM, C. S. & KLEIN, K. G. 2019 Solar wind temperature isotropy. *Phys. Rev. Lett*. **123** (14), 145101.

YU, J., WANG, J., LI, L. Y., CUI, J., CAO, J. B. & HE, Z. G. 2020 Electron diffusion by coexisting plasmaspheric hiss and chorus waves: multisatellite observations and simulations. *Geophys. Res. Lett*. **47** (15).

ZASLAVSKII, G. M., ZAKHAROV, M. I., NEISHTADT, A. I., SAGDEEV, R. Z. & USIKOV, D. A. 1989 Multidimensional Hamiltonian chaos. *Zh. Eksp. Teor. Fiz*. **96**, 1563–1586.

ZASLAVSKY, G. M. 2005 *Hamiltonian Chaos and Fractional Dynamics*. Oxford University Press.

ZASLAVSKY, A., KRAFFT, C., GORBUNOV, L. & VOLOKITIN, A. 2008 Wave-particle interaction at double resonance. *Phys. Rev.* E **77** (5), 056407.

ZELENYI, L. M. & MILOVANOV, A. V. 2004 Fractal topology and strange kinetics: from percolation theory to problems in cosmic electrodynamics. *Phys. Uspekhi* **47**, 749–788.

ZHANG, X. J., AGAPITOV, O., ARTEMYEV, A. V., MOURENAS, D., ANGELOPOULOS, V., KURTH, W. S., BONNELL, J. W. & HOSPODARSKY, G. B. 2020*a* Phase decoherence within intense chorus wave packets constrains the efficiency of nonlinear resonant electron acceleration. *Geophys. Res. Lett*. **47** (20), e89807.

ZHANG, X.-J., LI, W., THORNE, R. M., ANGELOPOULOS, V., BORTNIK, J., KLETZING, C. A., KURTH, W. S. & HOSPODARSKY, G. B. 2016 Statistical distribution of EMIC wave spectra: observations from Van Allen Probes. *Geophys. Res. Lett*. **43**, 12.

ZHANG, X. J., MOURENAS, D., ARTEMYEV, A. V., ANGELOPOULOS, V., BORTNIK, J., THORNE, R. M., KURTH, W. S., KLETZING, C. A. & HOSPODARSKY, G. B. 2019 Nonlinear electron interaction with intense chorus waves: statistics of occurrence rates. *Geophys. Res. Lett*. **46** (13), 7182–7190.

ZHANG, X. J., MOURENAS, D., ARTEMYEV, A. V., ANGELOPOULOS, V., KURTH, W. S., KLETZING, C. A. & HOSPODARSKY, G. B. 2020*b* Rapid frequency variations within intense chorus wave packets. *Geophys. Res. Lett*. **47** (15), e88853.

ZHANG, X.-J., MOURENAS, D., ARTEMYEV, A. V., ANGELOPOULOS, V. & THORNE, R. M. 2017 Contemporaneous EMIC and whistler mode waves: observations and consequences for MeV electron loss. *Geophys. Res. Lett*. **44**, 8113–8121.

ZHANG, X. J., THORNE, R., ARTEMYEV, A., MOURENAS, D., ANGELOPOULOS, V., BORTNIK, J., KLETZING, C. A., KURTH, W. S. & HOSPODARSKY, G. B. 2018 Properties of intense field-aligned lower-band chorus waves: implications for nonlinear wave-particle interactions. *J. Geophys. Res. (Space Phys.)* **123** (7), 5379–5393.

ZHENG, L., CHEN, L. & ZHU, H. 2019 Modeling energetic electron nonlinear wave-particle interactions with electromagnetic ion cyclotron waves. *J. Geophys. Res. (Space Phys.)* **124** (5), 3436–3453.

https://doi.org/10.1017/S0022377821000246 Published online by Cambridge University Press